AD-A075 210 NAVAL POSTGRADUATE SCHOOL MONTEREY CA F/G 20/5
FREQUENCY CONTROL OF A CO2 LASER USING STARK CELL STABILIZATION--ETC(U)
JUN 79 D M BROW

UNCLASSIFIED NL

1 OF 2
AD A075210

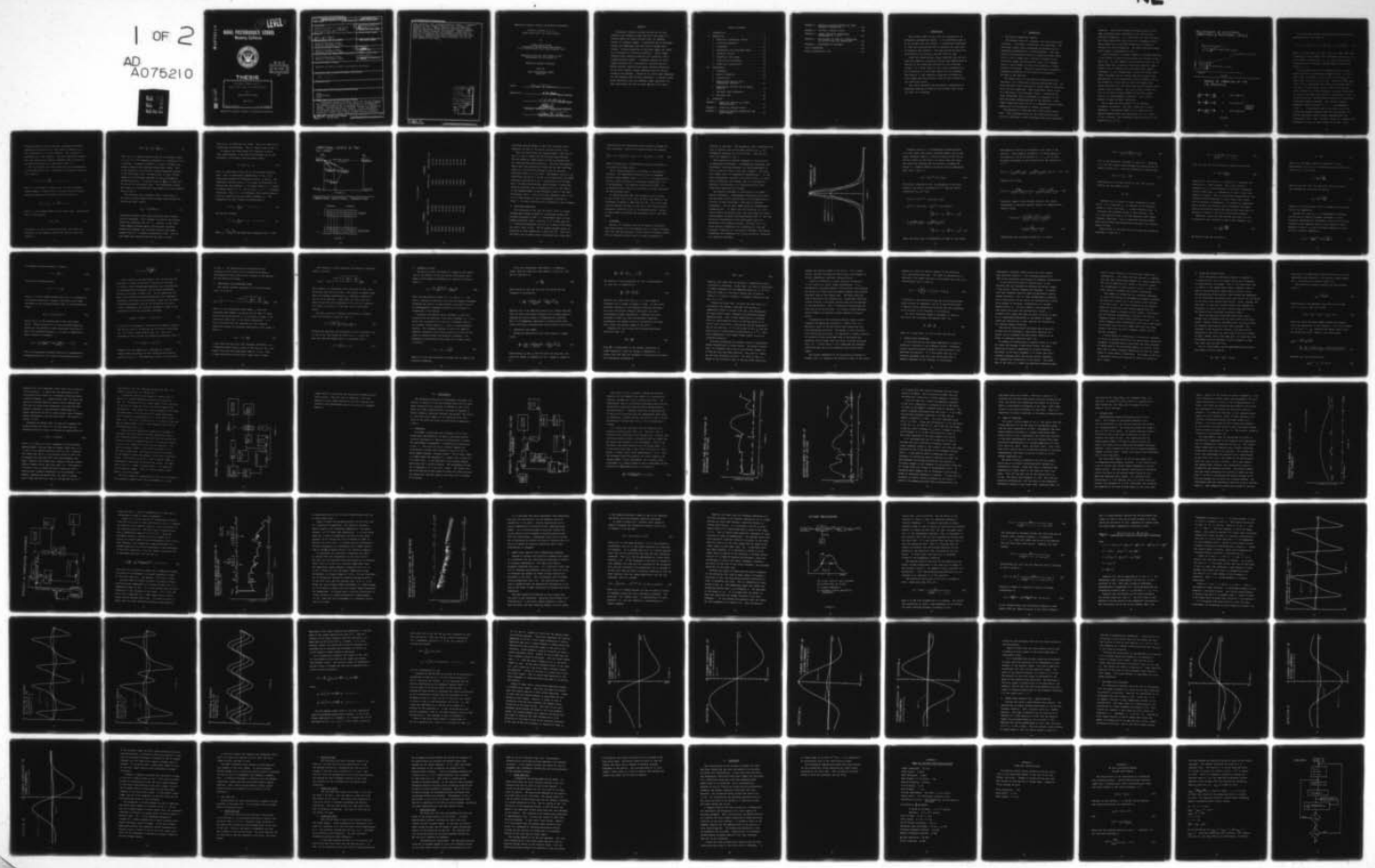

# NAVAL POSTGRADUATE SCHOOL

## Monterey, California




# THESIS

FREQUENCY CONTROL OF A $CO_2$
LASER USING STARK CELL STABILIZATION

by

Daniel Morris Brown

June 1979

Thesis Advisor: A. W. Cooper

SECURITY CLASSIFICATION OF THIS PAGE (When Data Entered)

## REPORT DOCUMENTATION PAGE

READ INSTRUCTIONS BEFORE COMPLETING FORM

1. REPORT NUMBER

2. GOVT ACCESSION NO.

3. RECIPIENT'S CATALOG NUMBER

4. TITLE (and Subtitle)

FREQUENCY CONTROL OF A $CO_2$ LASER USING STARK CELL STABILIZATION

5. TYPE OF REPORT & PERIOD COVERED

Master's Thesis; June 1979

6. PERFORMING ORG. REPORT NUMBER

7. AUTHOR(s)

Daniel Morris Brown

8. CONTRACT OR GRANT NUMBER(s)

9. PERFORMING ORGANIZATION NAME AND ADDRESS

Naval Postgraduate School
Monterey, California 93940

10. PROGRAM ELEMENT, PROJECT, TASK AREA & WORK UNIT NUMBERS

11. CONTROLLING OFFICE NAME AND ADDRESS

Naval Postgraduate School
Monterey, California 93940

12. REPORT DATE

June 1979

13. NUMBER OF PAGES

121

14. MONITORING AGENCY NAME & ADDRESS(if different from Controlling Office)

Naval Postgraduate School
Monterey, California 93940

15. SECURITY CLASS. (of this report)

Unclassified

15a. DECLASSIFICATION/DOWNGRADING SCHEDULE

16. DISTRIBUTION STATEMENT (of this Report)

Approved for public release; distribution unlimited.

17. DISTRIBUTION STATEMENT (of the abstract entered in Block 20, if different from Report)

18. SUPPLEMENTARY NOTES

19. KEY WORDS (Continue on reverse side if necessary and identify by block number)

Laser
Stabilization
Stark

20. ABSTRACT (Continue on reverse side if necessary and identify by block number)

Preliminary studies have been carried out for the frequency and intensity stabilization of the output of a Sylvania Model 941 Carbon Dioxide laser, by feedback control of resonator length. Fluctuations due to discharge current and temperature and flow rate of coolant were studied. Current regulation of the power supply was found to be necessary for intensity stability. Cavity length tuning allowed vibration-rotation

→ next page

DD FORM 1 JAN 73 1473 (Page 1)

EDITION OF 1 NOV 65 IS OBSOLETE
S/N 0102-014-6601

251 450

SECURITY CLASSIFICATION OF THIS PAGE (When Data Entered)

line selection, with a strong hysteresis effect. A computer analysis of error signal production for a pyroelectric detector and for a HgCdTe detector indicated that phase sensitive detection of the first harmonic signal component gave the typical frequency discriminant. Operation of a servo loop integrator for the feedback loop has been considered. A suitable Stark Effect absorption cell for feedback signal generation has been constructed, but has not been applied to the laser.

Approved for public release; distribution unlimited.

# FREQUENCY CONTROL OF A $CO_2$ LASER USING STARK CELL STABILIZATION

by

Daniel Morris Brown
Lieutenant, United States Coast Guard
B.S., United States Coast Guard Academy, 1975

Submitted in partial fulfillment of the
requirements for the degree of

MASTER OF SCIENCE IN PHYSICS

from the

NAVAL POSTGRADUATE SCHOOL
June 1979

Author Daniel M. Brown

Approved by: R. W. Cooper
Thesis Advisor

E. R. Crittenden, Jr.
Second Reader

Chairman, Department of Physics and Chemistry

William M. Tolles
Dean of Science and Engineering

## ABSTRACT

Preliminary studies have been carried out for the frequency and intensity stabilization of the output of a Sylvania Model 941 Carbon Dioxide laser, by feedback control of resonator length. Fluctuations due to discharge current and temperature and flow rate of coolant were studied. Current regulation of the power supply was found to be necessary for intensity stability. Cavity length tuning allowed vibration-rotation line selection, with a strong hysteresis effect. A computer analysis of error signal production for a pyroelectric detector and for a HgCdTe detector indicated that phase sensitive detection of the first harmonic signal component gave the typical frequency discriminant. Operation of a servo loop integrator for the feedback loop has been considered. A suitable Stark Effect absorption cell for feedback signal generation has been constructed, but has not been applied to the laser.

TABLE OF CONTENTS

# I. INTRODUCTION

The Sylvania Model 941 $CO_2$ laser was purchased to do atmospheric propagation studies. It was determined then to be too unstable for such studies. A program was undertaken to study the instabilities and to stabilize the laser both in frequency and intensity. The novel method of Stark cell stabilization was chosen as the best route to take.

Stark cell stabilization, being relatively new, has not come into commercial production but has been demonstrated as feasible in the laboratory and used on a few prototype systems. As a result there is very little information in the literature as to the exact details of the technique. Particularly, it was required to know how to produce an error signal and which detector would be most suitable for the stabilized system.

This thesis describes the preliminary accumulation of knowledge required to stabilize the Sylvania laser using the Stark cell technique.

## II. THEORETICAL

### A. ROTATIONAL-VIBRATIONAL SPECTRA

The quantum states of a molecule arise from three types of motion : electronic, vibrational, and rotational. The electronic charge cloud surrounding the molecule may be represented mathematically by wave functions. This wave function representation results in quantized energy states just as with a single atom. Motions or changes in the electronic charge distribution may result in a changing electric dipole moment in which case radiation is either absorbed or released. Electronic transitions correspond to frequencies primarily in the visible and ultraviolet portions of the spectrum.

The atomic nuclei in the molecule themselves are not stationary, but vibrate about some equilibrium position. For each electronic level there may be several modes of vibration which are also quantized. These vibrational levels result in a splitting of the electronic levels. Transitions between vibrational levels correspond to frequencies in the near and middle infrared portions of the spectrum. Vibrational transitions which result in a changing electric dipole moment occur via absorption or release of photons.

The molecule as a whole may also rotate about various axes. This rotational motion is also quantized and gives rise to a splitting of each vibrational level into rotational

sublevels. Transitions between rotational levels of the same vibrational state correspond to far infrared and microwave frequencies. As in the other two types of motion only those transitions which result in a changing electric dipole moment will occur with absorption or release of radiation at these frequencies. The above described energy level scheme is represented by Fig. 1.

Carbon dioxide is a linear, symmetric, triatomic molecule. It can vibrate in three different modes as pictured in Fig. 2. These are: $v_1$, the symmetric stretch mode in which the two oxygen atoms move in opposite directions along the longitudinal line of symmetry while the carbon atom remains stationary; $v_2$, the bending mode in which the oxygen atoms remain stationary and the carbon atom moves along a line perpendicular to the longitudinal line of symmetry; and $v_3$, the asymmetric stretch mode in which the oxygen atoms remain stationary and the carbon atom moves along the longitudinal line of symmetry. Only the $v_2$ and $v_3$ modes give rise to an electric dipole moment and can thus couple directly to electromagnetic radiation. The $v_1$ motion appears strongly in Raman scattering.

The $v_2$ mode can occur equally in two different orthogonal directions. Thus the $v_2$ mode has a twofold degeneracy. The quantum number $\ell$ is a measure of the angular momentum about the longitudinal axis as a result of the $v_2$ motion. The vibrational quantum states are then denoted by $[v_1\ v_2^{\ell}\ v_3]$.

# RELATIONSHIP OF ELECTRONIC, VIBRATIONAL & ROTATIONAL LEVELS

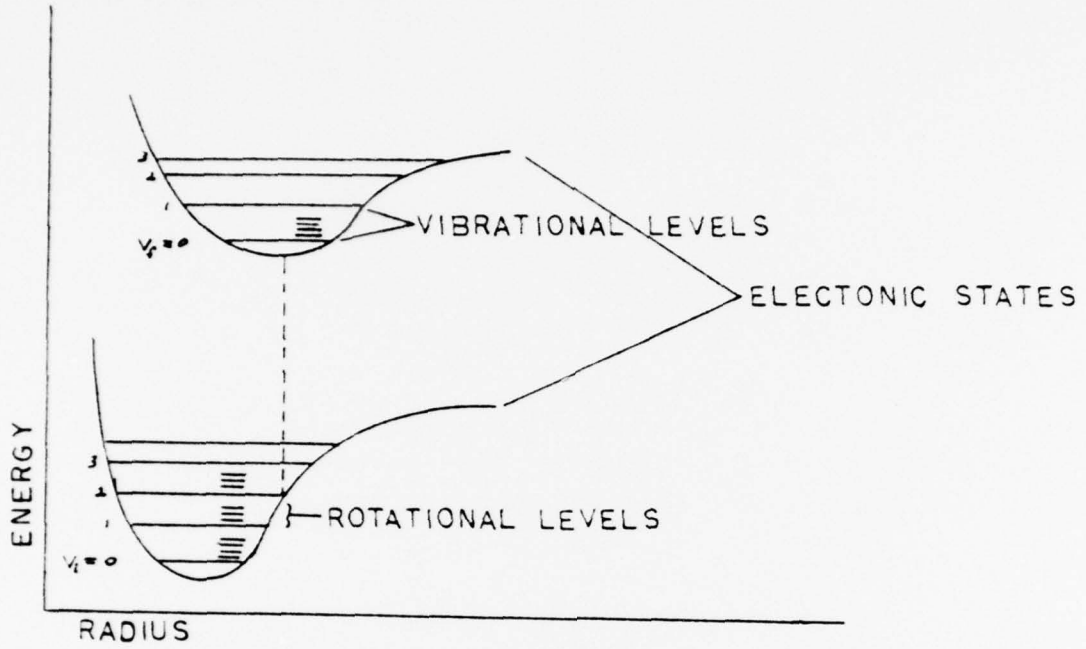


FIGURE 1

# MODES OF VIBRATION OF THE $CO_2$ MOLECULE

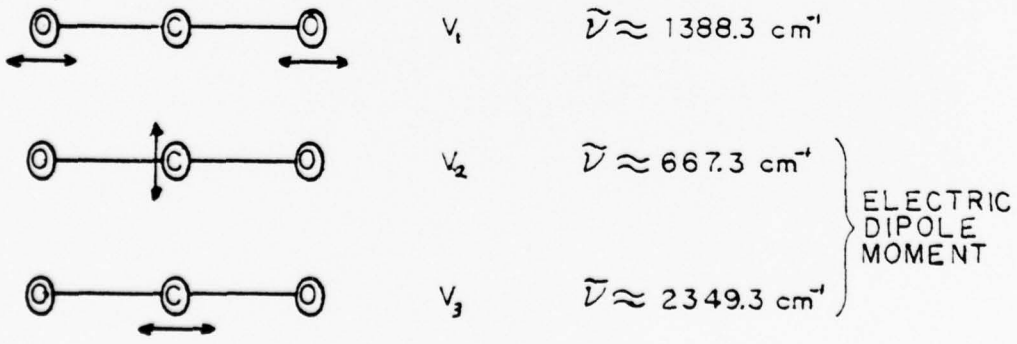


FIGURE 2

The vibrational energy associated with a given state is approximated to first order by

$$E_v = (v_1 + \tfrac{1}{2})\, hc\tilde{\nu}_1 + (v_2 + \tfrac{1}{2})\, hc\tilde{\nu}_2 + (v_3 + \tfrac{1}{2})\, hc\tilde{\nu}_3 \qquad (1)$$

where $\tilde{\nu}_1 \cong 1388.3\ cm^{-1}$, $\tilde{\nu}_2 \cong 667.3\ cm^{-1}$, $\tilde{\nu}_3 \cong 2349.3\ cm^{-1}$, the frequencies in wave number units associated with the $v_1$, $v_2$, and $v_3$ modes, respectively. $v_1$, $v_2$, and $v_3$ in the above equation are the vibrational quantum numbers and take on values 0, 1, 2, ... .

The $CO_2$ energy levels of principal interest in laser action and their corresponding frequencies are: [00°1] at 2349.3 $cm^{-1}$, $[10^{\circ}0,02^{\circ}0]_I$ at 1388.3 $cm^{-1}$, $[10^{\circ}0,02^{\circ}0]_{II}$ at 1285.5 $cm^{-1}$, and $[01^{1}0]$ at 667.3 $cm^{-1}$. The $[10^{\circ}0,02^{\circ}0]_I$ and $[10^{\circ}0, 02^{\circ}0]_{II}$ representations follow the notation used by Tyte [Ref. 1] and signify the fact that the [10°0] and [02°0] levels are in Fermi resonance. The main transitions of interest and these four levels are represented in Fig. 3. In the figure the $\Sigma$ and $\Pi$ notations refer to the electronic-vibrational angular momentum. This vibronic angular momentum K takes on values 0, 1, 2 ... corresponding to $\Sigma$, $\Pi$, $\Delta$ ... , respectively and is the vector sum of the vibrational angular momentum about the internuclear axis and the electronic orbital angular momentum about the internuclear axis. The $\Sigma$, $\Pi$, and $\Delta$ states of a molecule are analogous to the s, p, and d states of an atom. The g

subscript denotes that the vibronic eigenfunction remains unchanged upon reflection at the center of symmetry, i.e., the eigenfunction is of even symmetry. The u denotes an eigenfunction of odd symmetry. The plus superscript denotes that the eigenfunction remains unchanged when reflected at any plane containing all of the nuclei [Ref. 2].

The $CO_2$ molecule can rotate about any axis perpendicular to the longitudinal axis. The energy of rotation is given to first order by

$$E_J = J(J + 1) \frac{\hbar^2}{2I} \qquad J = 0, 1, 2, \ldots \tag{2}$$

where I is the moment of inertia and J is the rotational quantum number. From Eq.(2) it is observed that the energy difference between two adjacent rotational states is

$$\Delta E_J = E_{J+1} - E_J = \frac{\hbar^2}{I} (J + 1) \tag{3}$$

where J is the quantum number of the lower state. Substituting into (3) the equation

$$\Delta E_J = \frac{hc}{\lambda} \quad , \tag{4}$$

solving for $1/\lambda$ the reciprocal wavelength, and taking the difference in wave numbers between the spectral lines one arrives at

$$\Delta\left(\frac{1}{\lambda}\right) = \frac{1}{\lambda_1} - \frac{1}{\lambda_2} = \frac{\hbar}{2\pi cI}\,\Delta J \quad . \tag{5}$$

From (5) it is clearly observed that for two adjacent lines, i.e., $\Delta J = \pm 1$, the frequency difference is a constant if I is a constant. In general, however, I is not a constant, but changes slightly with different vibrational states. This is the reason for the observed slightly nonuniform spacing of the rotational lines. Herzberg [Ref. 2] gives various values of the rotational constant for the corresponding vibrational levels. A typical value for $\frac{\hbar}{4\pi Ic}$ is 0.3899 $cm^{-1}$ for the $[01^{1}0]$ vibrational level. This nonuniform spacing also shows up in the departure from parabolic of the potential curve in Fig. 1.

The selection rules originate from a calculation of the electric dipole moment matrix element taken between the initial and final states;

$$p_{fi} = \left|\int \psi_f^{*}\, e\vec{r}\,\psi_i\, d\tau\right| \quad . \tag{6}$$

Transitions between states which yield the above integral zero are forbidden. For a harmonic oscillator the integral yields the selection rule $\Delta v = \pm 1$. However, as the vibrational energy increases and/or the molecular structure becomes more complex, the vibration departs from simple harmonic and $\Delta v = \pm 1$ cannot be expected to hold. From (6) also comes the selection rule for $CO_2$ that a u state

must go to a g state and vice versa. But u to u and g to g transitions are forbidden. This is clearly seen in Fig. 3.

In general the total energy of a molecule to first order approximation is the sum of the energies due to the electronic, vibrational, and rotational states;

$$E = E_e + E_v + E_J \tag{7}$$

The I.R. transitions of $CO_2$ are of the vibration-rotation type. This is represented schematically in Fig. 4 for transitions between two vibrational levels, $v_i$ and $v_f$. The rotational selection rule $\Delta J = \pm 1$ causes the spectrum to be divided into two branches: a "P branch" where $\Delta J = +1$ and an "R branch" where $\Delta J = -1$. For $CO_2$ this is a $\Sigma^+ - \Sigma^+$ vibronic transition. Thus $\Delta J = 0$ is forbidden, which would otherwise yield a Q branch at the band center frequency $\nu_o$. The frequencies for the P branch are represented by

$$\nu \cong \nu_o - \frac{h}{4\pi^2 I} J \qquad J = 2, 4, 6 \ldots \tag{8}$$

and for the R branch

$$\nu \cong \nu_o + \frac{h}{4\pi^2 I} (J + 1) \qquad J = 0, 2, 4 \ldots \tag{9}$$

where $\nu_o = \frac{E_{v_i} - E_{v_f}}{h}$ the band center frequency and J is the

# VIBRATIONAL LEVELS OF THE $CO_2$ LASER

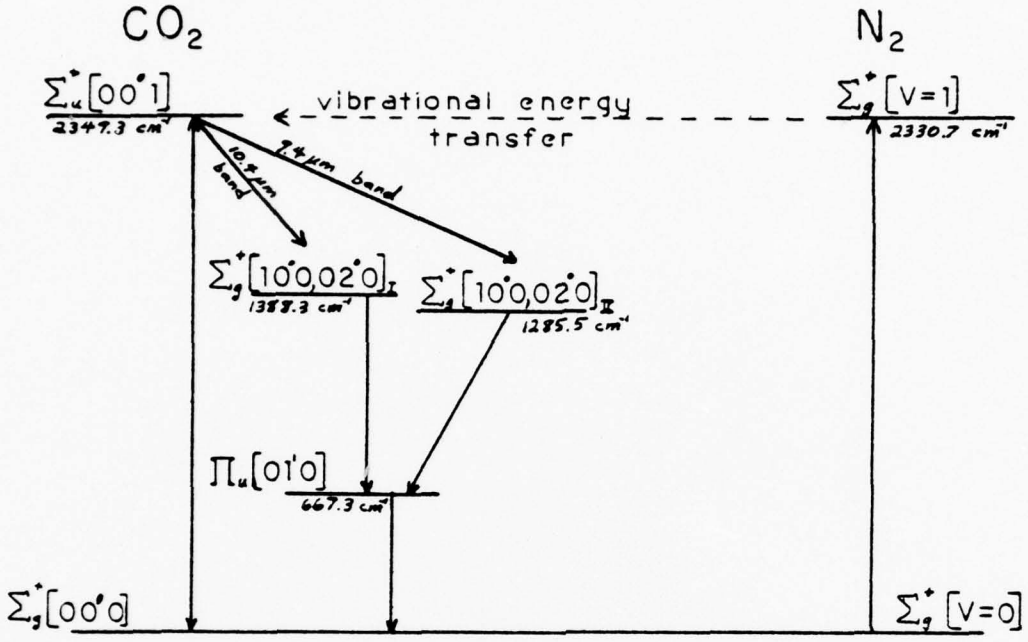


FIGURE 3

# VIBRATIONAL ROTATIONAL TRANSITIONS

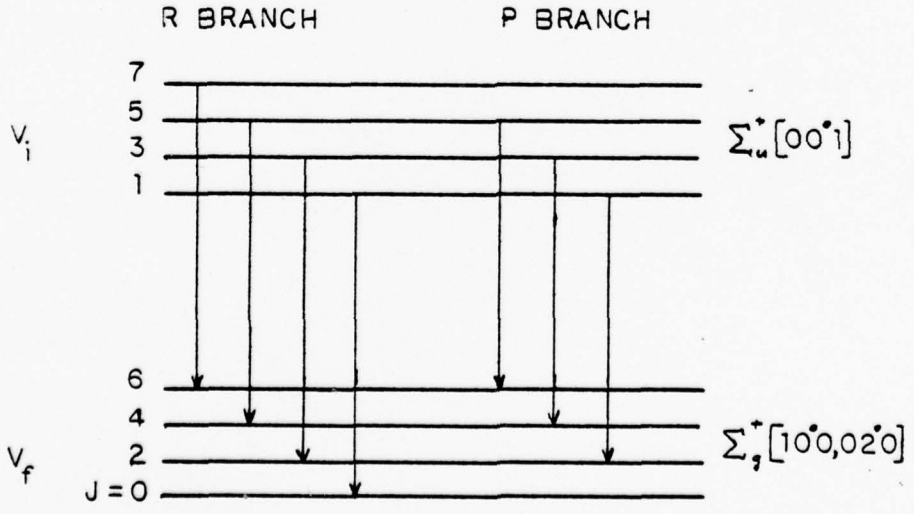


FIGURE 4

10.4 μm Band

| R branch | | P branch | |
|---|---|---|---|
| Rotation Line | Wavelength (μm) | Rotation Line | Wavelength (μm) |
| R(12) | 10.304 | P(12) | 10.513 |
| R(14) | 10.289 | P(14) | 10.532 |
| R(16) | 10.275 | P(16) | 10.551 |
| R(18) | 10.260 | P(18) | 10.571 |
| R(20) | 10.247 | P(20) | 10.591 |
| R(22) | 10.233 | P(22) | 10.611 |
| R(24) | 10.220 | P(24) | 10.632 |
| R(26) | 10.207 | P(26) | 10.653 |
| R(28) | 10.195 | P(28) | 10.675 |
| R(30) | 10.182 | P(30) | 10.696 |

Table I

rotational quantum number in the lower vibration level. Equations (8) and (9) are easily derived from Eq. (2).

Note the values which the quantum number J may take on. $CO_2$ is a linear symmetrical (point group $D_{\infty h}$) molecule. The two identical oxygen nuclei in the $CO_2$ molecule have zero spin and obey Bose statistics. Thus all antisymmetric levels have zero statistical weight and the odd rotational levels of a $\Sigma_g^+$ state are missing as well as the even rotational levels of a $\Sigma_u^+$ state. Consequently the $\Sigma_u^+$ to $\Sigma_g^+$ transitions for the 10.4 μm and 9.4 μm bands have the simple structure illustrated in Fig. 4 consisting of an R branch and a P branch with alternate lines missing. A particular vibration-rotation line is denoted by P(J) or R(J) where J is the quantum number of the rotational level in the lower vibrational state. A few of the more important lines in the 10.4 μm band along with their wavelengths are given in Table 1. Of these lines the P(20) transition is the strongest.

## B. EXCITATION MECHANISM

The excitation of $CO_2$ into the [00°1] level is readily accomplished through transfer of vibrational energy from nitrogen molecules in the v = 1 vibrational level of their ground electronic state. From Fig. 3 it is seen that the v = 1 excited vibrational level of $N_2$ is about 19 $cm^{-1}$ below the [00°1] level of $CO_2$. The kT average thermal energy of molecules at room temperature is about 210 $cm^{-1}$. Thus these two levels are in almost exact coincidence and a high cross

section exists for vibrational energy transfer through two-body collisions. This may be represented by the equation

$$N_2^*(v = 1) + CO_2(00°1) \rightarrow N_2(v = 0) + CO_2(00°1) - 19\ cm^{-1} \qquad (10)$$

where $N_2^*$ represents a vibrationally excited $N_2$ molecule in the ground electronic state.

$N_2^*$ is easily produced by a discharge in low pressure nitrogen. The homonuclear molecule $N_2$ has no permanent electric dipole moment; thus a v = 1 to v = 0 transition via electric dipole radiation is forbidden, causing $N_2^*(v = 1)$ to be metastable. The downward transition for $N_2^*(v = 1)$ is governed almost solely by collisions with other molecules and the container walls.

It should be noted that the excitation cross section of $CO_2$ to the [10°0, 02°0] level by $N_2^*$ is very small as the difference in energy is more than 900 $cm^{-1}$. This fact along with the shorter lifetime of the [10°0, 02°0] level allows a population inversion in $CO_2$ to be achieved easily. Helium is often added to increase the relaxation rate of the lower level.

## C. LINESHAPES

Analysis of a spectral line of an atomic or molecular transition reveals it to be composed not of a single frequency only, but that the line has a finite width or frequency spread with an intensity profile which is either Lorentzian or

Gaussian in the limit. The frequencies form a continuum from zero to infinity with the maximum intensity at $\nu_o$, the fundamental frequency of the transition. These two profiles are compared in Fig. 5.

The Lorentzian or natural lineshape is characteristic of homogeneous broadening. In homogeneous broadening, the absorbing or emitting molecules are indistinguishable as they all absorb or emit at the same frequency. The three most common causes of homogeneous broadening are: (1) the finite spontaneous lifetime of an excited state, (2) collisions of molecules with phonons, and (3) collisions of molecules with molecules in a high-pressure gas which effectively decreases the lifetime.

The Gaussian lineshape is characteristic of inhomogeneous broadening. Inhomogeneous broadening occurs when the absorbing or emitting molecules are distinguishable as a result of their absorbing or emitting at different frequencies. The two most common causes of inhomogeneous broadening are: (1) impurities and variations in a host crystal affect the energy levels and thus change the transition frequency of nearby emitting molecules and (2) the high velocities encountered in hot plasma gases cause the frequencies to be Doppler-shifted. Obviously for a $CO_2$ laser pressure broadening will predominate at high gas pressures, resulting in a Lorentzian lineshape, and Doppler broadening will predominate at low gas pressures, resulting in a Gaussian lineshape.

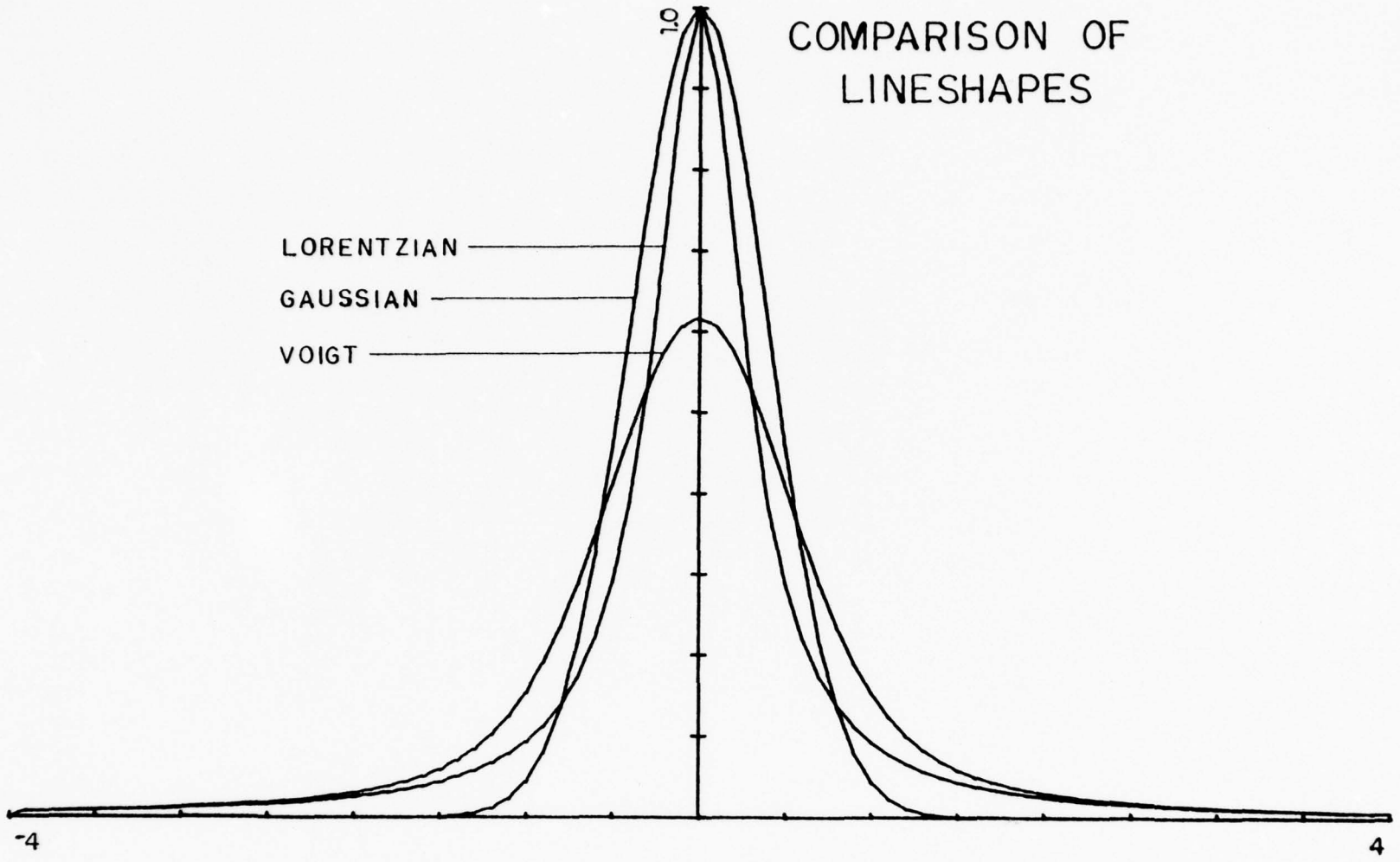


FIGURE 5

Consider cause No. 1 of homogeneous broadening above. It is well known from Fourier transform theory that a pure single frequency implies a transition which occurs over an infinite amount of time which, of course, does not occur. The Lorentzian lineshape may be derived by assuming the emitter is a damped harmonic oscillator with an exponential decay time $\tau$ [Ref. 3].

$$\varepsilon(t) = E_o e^{-t/\tau} \cos 2\pi\nu_o t \tag{11}$$

The Fourier transform of (11) is equivalent to the convolution of the Fourier transform of $e^{-t/\tau}$ and the Fourier transform of $E_o \cos 2\pi\nu_o t$:

$$F\{\varepsilon(t)\} = F\{e^{-t/\tau}\} * F\{E_o \cos 2\pi\nu_o t\}$$

$$= \left[\int_0^\infty e^{-t/\tau} \cos 2\pi\nu t dt - i\int_0^\infty e^{-t/\tau} \sin 2\pi\nu t dt\right] * \left[\frac{E_o}{2}\delta(\nu - \nu_o) + \frac{E_o}{2}\delta(\nu + \nu_o)\right]$$

$$= \left[\frac{1/\tau}{(1/\tau)^2 + 4\pi^2\nu^2} - \frac{i2\pi\nu}{(1/\tau)^2 + 4\pi^2\nu^2}\right] * \left[\frac{E_o}{2}\delta(\nu - \nu_o) + \frac{E_o}{2}\delta(\nu + \nu_o)\right] \tag{12}$$

where the lower limit of integration is taken as zero rather

than negative infinity to correspond to the start of the emission. Since negative frequencies are being ignored in this analysis, the delta function at $\nu = +\nu_o$ in (12) may be taken with height $E_o$ and convolved with the transform of $e^{-t/\tau}$:

$$F\{\varepsilon(t)\} = \left[\frac{1/\tau}{(1/\tau)^2 + 4\pi^2\nu^2} - \frac{i2\pi\nu}{(1/\tau)^2 + 4\pi^2\nu^2}\right] * [E_o\ \delta(\nu - \nu_o)] \quad (13)$$

Equation (13) yields:

$$F\{\varepsilon(t)\} = \frac{(1/\tau)E_o}{(1/\tau)^2 + 4\pi^2(\nu - \nu_o)^2} - \frac{i2\pi(\nu - \nu_o)E_o}{(1/\tau)^2 + 4\pi^2(\nu - \nu_o)^2} \quad . \quad (14)$$

Taking the square of the absolute value of (14) (which corresponds to the power spectral density in communications theory) yields:

$$|F\{\varepsilon(t)\}|^2 = \frac{(1/\tau)^2 E_o^{\ 2} + 4\pi^2(\nu - \nu_o)^2 E_o^{\ 2}}{[(1/\tau)^2 + 4\pi^2(\nu - \nu_o)^2]^2}$$

$$= \frac{E_o^{\ 2}}{(1/\tau)^2 + 4\pi^2(\nu - \nu_o)^2} \quad (15)$$

Normalizing (15) according to $\int_{-\infty}^{\infty} g(\nu)d\nu = 1$ yields

$$g(\nu) = \frac{2/\tau}{(1/\tau)^2 + 4\pi^2(\nu - \nu_o)^2} \quad . \tag{16}$$

This is the Lorentzian lineshape in terms of $\tau$. Defining $\Delta\nu$ as the full width at half maximum the Lorentzian may be found in terms of $\Delta\nu$. From the definition it follows that

$$g(\nu_o)/2 = g(\nu_o + \frac{\Delta\nu}{2}) \quad . \tag{17}$$

Substituting in the proper values of (16) into (17) and carrying out the algebra yields

$$\frac{1}{\tau} = \pi\Delta\nu \quad . \tag{18}$$

Equation (18) is worthy of closer examination at this point. It is noted that $\Delta\nu$ is a measure of the frequency spread or finite line width. $\tau$ is the transition time. As $\tau$ decreases the frequency spread $\Delta\nu$ must increase. Only if $\tau$ were infinite would $\Delta\nu$ be zero implying a pure single frequency transition. This is consistent with the remark made earlier concerning transitions occurring in an infinite amount of time.

Substitution of (18) back into (16) yields the Lorentzian lineshape in terms of $\Delta\nu$:

$$g(\nu) = \frac{\Delta\nu}{2\pi\left[\left(\frac{\Delta\nu}{2}\right)^2 + (\nu - \nu_o)^2\right]} \quad . \tag{19}$$

From (18) and (19) the following is observed to be true:

$$\Delta\nu = \frac{1}{\pi\tau} = \frac{2}{\pi g(\nu_o)} \tag{20}$$

Equation (20) says that as $\Delta\nu$ increases or $\tau$ decreases the intensity at $\nu_o$ must decrease. But if the intensity decreases at $\nu_o$ it also decreases at all other frequencies within a region near $\nu_o$, frequencies at which a laser will normally oscillate. This is one possible explanation for the typically observed decrease in power output from a laser with an increase in temperature. An increase in temperature would increase the pressure without increasing the number density and pressure broaden the gain profile resulting in a decrease in output at the cavity oscillation frequency.

Reference 4 gives the time between collisions in a gas at pressure p for a molecule of mass M and a diameter a as

$$\tau_p \cong \frac{1}{pa^2}\sqrt{\frac{MkT}{16\pi}} \tag{21}$$

The universal gas law is given as

$$p = NkT \tag{22}$$

where N is the number density of molecules in a gas. Substituting (22) into (21) and defining the collision cross section as $Q = \pi a^2$ yields

$$\tau_p = \frac{1}{NQ}\sqrt{\frac{M\pi}{16kT}} \tag{23}$$

Substituting (23) into (20) then gives the full width at half maximum due to pressure broadening

$$\Delta\nu_p = \frac{NQ}{\pi}\sqrt{\frac{16kT}{M\pi}} \tag{24}$$

Equation (24) clearly shows that $\Delta\nu$ increases as the square root of the temperature.

Consider now cause no. 2 of inhomogeneous broadening. The Gaussian or Doppler broadened lineshape is easily derived by beginning with the Maxwell velocity distribution function in one dimension which is the probability that a molecule of mass M in a gas at average temperature T will have an x velocity component $v_x$

$$\phi(v_x) = \left[\frac{M}{2\pi kT}\right]^{1/2} \exp\left[\frac{-Mv_x^2}{2kT}\right]. \tag{25}$$

The Doppler-shifted frequency is given as

$$\nu = \nu_o + \frac{v_x}{c} \nu_o \tag{26}$$

which upon rearranging gives

$$v_x = (\nu - \nu_o) \frac{c}{\nu_o} \tag{27}$$

Since $\nu$ is also a random variable and $\phi(v_x)$ is a probability distribution function, a change of variables can be made according to the following formula [Ref. 5] from probability theory

$$g(\nu) = \phi(v_x) |J(v_x/\nu)| \tag{28}$$

where $J(v_x/\nu)$ is the Jacobian and in this case equals $dv_x/d\nu$. Using (25) and (27) in (28) and normalizing one arrives at the probability that a molecular oscillator of mass M and resonant frequency $\nu_o$ in a gas at temperature T emits a photon at frequency $\nu$

$$g(\nu) = \frac{c}{\nu_o} \left[\frac{M}{2\pi kT}\right]^{1/2} \exp\left[\frac{-Mc^2}{2kT\nu_o^2} (\nu - \nu_o)^2\right] \tag{29}$$

This is the Gaussian lineshape function for inhomogeneous broadening and has a full width at half maximum given by

$$\Delta\nu_D = 2\nu_o \sqrt{\frac{2kT \ln 2}{Mc^2}} \tag{30}$$

It was stated at the beginning of this section that the lineshape is either Lorentzian or Gaussian in the limit. In reality several broadening mechanisms occur simultaneously including Stark broadening, van der Waals broadening, and wall collisions to name a few. In the simplified case where two different broadening mechanisms yield comparable linewidths, but which are considerably larger than all other broadening mechanisms, and the two mechanisms are statistically independent, the observed lineshape is equal to the convolution of the two individual lineshapes

$$g_{obs}(\nu) = \int_0^\infty g_1(\nu - \nu')g_2(\nu')d\nu' \tag{31}$$

If one of the lineshapes is Gaussian due to Doppler broadening and the other is Lorentzian due to pressure broadening, Eq. (31) yields a Voigt profile [Ref. 6]. The total linewidth in this case may be estimated according to [Ref. 7]

$$\Delta\nu \approx [(\Delta\nu_D)^2 + (\Delta\nu_p)^2]^{1/2} \tag{32}$$

Equation (31) was numerically calculated on a Hewlett-Packard 9810A calculator for the Lorentzian and Gaussian profiles in Fig. 5. The normalized result is also plotted

in Fig. 5. All three profiles were plotted by the calculator on the same scale for comparison purposes. The program for the Voigt profile is given in the appendix for the inquisitive reader.

## D. LONGITUDINAL AND TRANSVERSE MODES

The natural resonant frequency of a laser oscillator cavity is given by

$$\nu_{q\ell m} = \left[ q + (\ell + m + 1) \frac{\cos^{-1} \sqrt{(1 - \frac{L}{R_1})(1 - \frac{L}{R_2})}}{\pi} \right] \frac{c}{2nL} \qquad (33)$$

where q is the longitudinal mode number, $\ell$ and m are transverse mode numbers, $R_1$ and $R_2$ are the radii of curvature of the cavity mirrors, c is the speed of light, n the refractive index, and L is the mirror separation. It is easily verified from this equation that the frequency separation between two adjacent longitudinal cavity modes is given by

$$\nu_{q+1} - \nu_q = \frac{c}{2nL} \qquad (34)$$

A laser which has gain over this frequency difference, i.e., a linewidth greater than or equal to the value of (34), will support more than one longitudinal mode at a time. Thus a single mode device should have a short cavity length.

The frequency or mode separation for adjacent transverse modes is given by

$$\nu_{\ell+m+1} - \nu_{\ell+m} = \left[ \frac{\cos^{-1} \sqrt{(1 - \frac{L}{R_1})(1 - \frac{L}{R_2})}}{\pi} \right] \frac{c}{2nL} \qquad (35)$$

This quantity is considerably less than that of (34), and often less than the line width. The problem of higher order modes oscillating simultaneously is sometimes remedied by the use of an aperture. Bloom [Ref. 8] states that the lowest order mode will predominate for laser bore diameters less than $3.5 \times \omega$ where $\omega$ is the spot size on the output mirror.

The spot size for a resonator with mirrors of unequal radii of curvature is given by [Ref. 9]

$$\omega_1^4 = \left[ \frac{\lambda R_1}{\pi} \right]^2 \frac{R_2 - L}{R_1 - L} \frac{L}{R_1 + R_2 - L} \qquad (36)$$

Dividing the numerator and denominator on the right-hand side of (36) by $R_1^2$ and taking the limit as $R_1 \to \infty$ gives the spot size when the output mirror is an optical flat;

$$\omega_1^4 = \left( \frac{\lambda}{\pi} \right)^2 (R_2 - L) L \qquad (37)$$

## E. FREQUENCY PULLING

The passive cavity linewidth for R equal to the square root of the product of the two mirror reflectances and $\alpha$ equal to the average distributed loss constant is given by [Ref. 3]

$$\Delta\nu_c = \frac{c[\alpha - \frac{1}{L} \ln R]}{2\pi n} \approx \frac{c(1 - R)}{2\pi nL} \tag{38}$$

where the approximation holds for $\alpha = 0$ and $R \approx 1$. The cavity linewidth is generally less than the Doppler broadened linewidth and results in hole burning in the gain curve of an inhomogeneously broadened system at the frequency or frequencies of oscillation.

In general the passive cavity resonance $\nu_q$ does not coincide with the molecular line center frequency $\nu_o$. As a result the oscillation will occur at a frequency near $\nu_q$ but slightly shifted toward $\nu_o$. This is called frequency pulling. This frequency pulling is due to the negative anomalous dispersion curve which results in a shift in the index of refraction near the molecular resonance. The frequency of oscillation of the laser for a high Q cavity is given by

$$\nu = \nu_q - (\nu_q - \nu_o)\frac{\Delta\nu_c}{\Delta\nu} \tag{39}$$

where $\Delta\nu$ is the total molecular linewidth due to Doppler and pressure broadening.

Since the longitudinal mode number q is immensely larger than the transverse mode numbers ℓ and m, Eq. (33) may be simplified to

$$\nu_q = \frac{qc}{2nL} \tag{40}$$

Substitution of (38) and (40) into (39) gives for the frequency of oscillation

$$\nu = \frac{qc}{2nL} - \left[\frac{qc^2(1 - R)}{4\pi n^2 L^2} - \frac{\nu_o c(1 - R)}{2\pi nL}\right]\frac{1}{\Delta\nu} \tag{41}$$

Equation (41) is an important result as it reveals the fact that the laser oscillation frequency may be tuned simply by changing the cavity length or broadening the linewidth. This is of fundamental importance in stabilization techniques utilizing a piezoelectric driven mirror in the cavity.

F. INSTABILITY AND CAUSES

Taking the derivative of (41) with respect to length yields

$$\frac{d\nu}{dL} = \frac{-qc}{2nL^2} + \left[\frac{qc^2(1 - R)}{2\pi n^2 L^3} - \frac{\nu_o c(1 - R)}{2\pi nL^2}\right]\frac{1}{\Delta\nu} \tag{42}$$

Substituting $\Delta\nu_c$ and $\nu_q$ from (38) and (40) back into (42) gives the change in frequency $d\nu$ for a change in length dL as

$$\frac{d\nu}{dL} = \frac{-\nu_q}{L} + \frac{1}{L}(2\nu_q - \nu_o)\frac{\Delta\nu_c}{\Delta\nu} \tag{43}$$

The quantity in the parentheses of (43) is approximately $\nu_q$; thus (43) is simplified to

$$\frac{d\nu}{dL} = \frac{-\nu_q}{L} + \frac{\nu_q}{L}\frac{\Delta\nu_c}{\Delta\nu} \tag{44}$$

Equation (44) shows that when $\Delta\nu_c << \Delta\nu$ the change in frequency with a change in length is large. As the cavity linewidth increases or the molecular linewidth decreases the laser oscillation frequency fluctuates less with corresponding length fluctuations. Normally the cavity linewidth is much less than the molecular linewidth; consequently the primary sources of instability are those which affect the optical length of the cavity.

Equation (44) also yields the following approximate expression [Ref. 10]

$$\frac{d\nu}{\nu} = \frac{-dL}{L} \tag{45}$$

Since $\frac{dL}{L}$ is proportional to the thermal coefficient of linear expansion $\alpha$ times the change in temperature, it follows from (45) that the frequency of oscillation fluctuates with temperature according to

$$\frac{d\nu}{\nu} = -\alpha dT \qquad (46)$$

Equation (46) shows that an increase in temperature yields a decrease in frequency. Mocker [Ref. 11] gives a coefficient of linear expansion for low expansion quartz of $2 \times 10^{-8}/°C$. With this value of $\alpha$ the laser coolant must be held to within 1°C in order to achieve a frequency stability of one part in $5 \times 10^{7}$.

Bridges and Patel [Ref. 12] point out that there is a narrowing of the Doppler linewidth with decrease in temperature, which is evident from (30), and consequently one would expect better frequency discrimination between competing modes. Thus if mode competition is a problem where an interferometric device or grating cannot be inserted within the cavity, lowering the coolant temperature may be the solution. It is also stated in Ref. 12 that the optical gain is approximately proportional to $T^{-3/2}$. Thus lower temperatures yield higher output powers as well as increased stability.

Pressure fluctuations are another source of instability, though insignificant in sealed lasers. According to Mocker [Ref. 13] frequency shifts due to gas pressure changes of 5-8 MHz per torr have been observed. This shift is toward the red with increasing pressure. The shift is due to a change in the refractive index of the gas which effectively

changes the optical length of the cavity. For a sealed cavity, pressure fluctuations would result from changes in the gas temperature especially during warm up.

Acoustic vibration is a major source of instability. It also results in cavity length fluctuations. It is minimized by utilizing internal cavity mirrors and isolating the cavity as a whole from the support members with acoustic absorbers such as foam rubber pads. The whole laser may then be enclosed in an anechoic box. Significant vibration results from the circulating coolant water and fluctuations in the tap pressure. This is minimized by maintaining the flow rate as low as possible. Air cooled systems and motor driven choppers can generate copious amounts of acoustic noise.

Fluctuations in the excitation current result in both frequency and amplitude instability. Mocker [Ref. 13] observed a shift of 500-900 kHz/mA shift toward the blue with increasing excitation. The amount of shift decreases with increasing excitation. The amplitude or output intensity is observed to have an optimum value of excitation and decreases with a change from this value in either direction [Ref. 12]. A laser which is to be amplitude and frequency stabilized must have a well regulated and filtered power supply.

The current dependence of the oscillation frequency is probably due to a change in the refractive index of the active

medium as a result of density changes of the electrons, ions, and neutral molecules. The index of refraction as a function of the number densities of electrons ($N_e$), ions ($N_i$), and molecules ($N_m$) is given by

$$n_o = 1 - \frac{1}{2}\frac{N_e e^2}{m\varepsilon_o \omega^2} + 2\pi \sum_i \alpha_i N_i + 2\pi\alpha_m N_m \quad . \tag{47}$$

A reduction in the refractive index may arise from the more rapid creation of components such as CO and NO which have a smaller electric permittivity than $CO_2$ and thus contribute to an increase in the frequency of oscillation.

The total fractional change in frequency is equal to the sum of the fractional fluctuations [Ref. 10],

$$\frac{\Delta\nu}{\nu} = \frac{\Delta n}{n} + \frac{\Delta L}{L} \quad , \tag{48}$$

where $\Delta n$ is found from (47) and $\Delta L$ from (45) and (46).

## G. STABILIZATION TECHNIQUES

As was noted earlier the output amplitude of a laser is primarily a function of the discharge current. Therefore, current regulation should eliminate a major portion of the amplitude fluctuations. It is also noted that due to a frequency-dependent gain curve the output amplitude is somewhat dependent on the frequency of oscillation.

Consequently frequency stabilization will also produce some amplitude stability. The following discussion of some of the techniques used focuses on frequency stabilization.

In the above discussion of instabilities, it was observed that each fluctuation effected the optical length of the cavity, thereby changing the frequency. It follows then that frequency stability would be achieved by cavity length correction. This is often accomplished by mounting one or both morrors of the cavity on a piezoelectric crystal which expands or contracts in proportion to a voltage applied across it. An error signal is then produced by some method and drives the piezoelectric crystal. A suitable error signal must meet two basic criteria; it must be of a magnitude proportional to the amount of length correction required and it must indicate the direction of the required length correction.

The various stabilization techniques may be basically divided into two categories, those which stabilize to a passive cavity resonance and those which stabilize to an atomic or molecular transition [Ref. 14].

An example of stabilizing to a passive cavity is to pass the laser beam through a Fabry-Perot etalon, the plate separation of which is modulated at an audio frequency. The effect of the audio frequency is to dither the cavity resonance frequency about the desired optical frequency, thus changing the transmission of the etalon. The output beam of the etalon is a phase and amplitude modulated signal

which is then converted to an electrical signal with a photodetector. The signal from the detector is compared with the audio modulating frequency in a lock-in amplifier. The lock-in amplifier D.C. output is the error signal. The disadvantage of using a passive cavity is that it is still subject to thermal and acoustic fluctuations.

One example of stabilizing to a molecular resonance is to use the Lamb dip of the Doppler broadened lineshape. The Lamb dip or power dip is the result of hole burning in the gain curve. The laser frequency may be dithered about the dip and the laser output compared with the dithering signal to produce an error signal. This method has the inherent disadvantage of having a very narrow frequency region in which stabilization can occur. If the laser frequency should inadvertently drift out of the region of the power dip, the error signal would have the wrong polarity and force the laser frequency further from the desired resonance.

A better method of stabilizing to a molecular resonance is to use an external gas-filled cell whose center absorption frequency is dithered about a point near the laser frequency by application of an oscillating magnetic or electric field. This type of center frequency modulation utilizes the Zeeman effect or Stark effect, respectively. The output of the cell is then phase sensitively detected as before to produce an error signal.

## H. STARK CELL STABILIZATION

If an absorbing or radiating molecule is immersed in a strong electric field its energy levels and consequently its spectrum will be changed. This is the Stark effect and is similar to the Zeeman effect where a magnetic field is used as the perturbation rather than an electric field. The application of the electric field removes the degeneracy of the vibrational-rotational levels and results in a splitting of the levels into several other levels. Kelly, Francke, and Feld [Ref. 15] give the relevant energy level diagram for absorption of several $CO_2$ laser lines by $NH_2D$ and show the splitting of the vibrational-rotational levels.

There are many gases whose absorption peaks can be brought into coincidence with $CO_2$ laser lines by the Stark effect. Martin, Corcoran, and Smith [Ref. 16] give a table of different gases and the laser lines absorbed. The remainder of the discussion, however, will focus on the absorption of the P(20) $CO_2$ laser line in the 10.4 μm band by $NH_2D$. Brewer, Kelly, and Javan [Ref. 17] found that this coincidence could be obtained at field strengths of 3298 V/cm, 4404 V/cm, and 6604 V/cm.

The D.C. Stark effect can be represented from perturbation theory to first order by

$$E_m = E_m^\circ - \langle \psi_m | p \cdot \varepsilon_s | \psi_m \rangle \qquad (49)$$

where $E_m^\circ$ is the unperturbed energy of state m, $\psi_m$ is the unperturbed wave function, p the molecular dipole moment, and $\varepsilon_s$ the Stark field operator [Ref. 19].

The transition frequency between two Stark shifted levels is

$$\nu_{mn} = \frac{E_m - E_n}{h} \quad . \tag{50}$$

Substituting a time-dependent Stark field of the form $\varepsilon_s(t) = \varepsilon_s \cos \omega t$ into (49) yields

$$E_m(t) = E_m^\circ - \langle \psi_m | p \cdot \varepsilon_s | \psi_m \rangle \cos \omega t \tag{51}$$

where the cosine has been brought outside the integral since the integration is over distance. It is also assumed in (51) that $\omega << \nu_{mn}$; otherwise the energy levels could not follow the field. Equation (50) then becomes

$$\nu_{mn}(t) = \frac{E_m(t) - E_n(t)}{h}$$

$$= \frac{E_m^\circ - E_n^\circ + (\langle \psi_n | p \cdot \varepsilon_s | \psi_n \rangle - \langle \psi_m | p \cdot \varepsilon_s | \psi_m \rangle) \cos \omega t}{h} \tag{52}$$

Equation (52) can be rewritten as

$$\nu_{mn}(t) = \nu_o + \Delta\nu' \cos \omega t \ . \tag{53}$$

Equation (53) is an important result which will be used in a later analysis. It shows that the application of an oscillating field results in a frequency modulation about a center frequency $\nu_o$. Claspy and Pao [Ref. 18] solve the equation of motion using the density matrix approach and show that for Stark field frequencies less than the homogeneous linewidth $\Delta\nu$, the absorption coefficient is a single Lorentzian line with a time varying center frequency moving synchronously with the Stark field. The result is similar to (53).

Nussmeier and Abrams [Ref. 19] give the frequency difference between the P(20) 10.6 μm line center and the absorption center of $NH_2D$ as a function of applied field as

$$\delta = 2042 + 0.143|M|E \qquad (54)$$

where $\delta$ is in MHz, M is the z component of the rotational quantum number J and can take on integer values from -4 to 4, and E is the applied electric field in V/cm. Equation (54) shows that for M = ±4 an electric field of 3570 V/cm is required to bring the P(20) line into resonance with $NH_2D$. Equation (54) differs only slightly from the results found by Brewer, Kelly, and Javan [Ref. 17]. The quantity $0.143|M|$ in (54) is called the Stark tuning rate and is reported only slightly differently in the literature. For example, Tangonan and Abrams [Ref. 20] report a tuning rate of $NH_2D$ and the P(20) line of .564 MHz cm/V for M = 4

which gives 0.141 |M|, Johnston and Melville [Ref. 21] report a tuning rate of .568 MHz cm/V.

A proposed stabilization scheme is shown in Fig. 6, which is a slightly modified version of that given in Ref. 19. The Stark cell D.C. power supply biases one plate of the cell to bring the P(20) line into resonance with the $NH_2D$ gas. This occurs at a field strength of 3570 V/cm. The other plate is driven with an AC signal producing a field strength of approximately 150 V/cm at about 10 KHz [Ref. 19]. The cell is filled with a 1:1 mixture of $ND_3$ and $NH_3$ at approximately 2 torr. The exchange occurs rapidly to produce $NH_2D$ [Ref. 21].

A beam splitter reduces the radiant flux incident on the Stark cell below $1 W/cm^2$ to avoid saturation effects. The transmitted intensity is then detected with an SBN pyroelectric detector or HgCdTe detector. The detector output is fed to the "signal in" on the lock-in amplifier. The audio oscillator signal is fed to the "reference in" on the lock-in amplifier. The lock-in determines the phase of the detector signal with respect to the audio oscillator input. The polarity of the D.C. lock-in output signal is determined by the phase of the detector signal. The amplitude of the D.C. output is proportional to the amplitude of the detector signal. The D.C. lock-in output signal then is the error signal.

The error signal is integrated over time in the integrator. The integrator output drives the programmable D.C. power

# STARK CELL STABILIZATION SCHEME

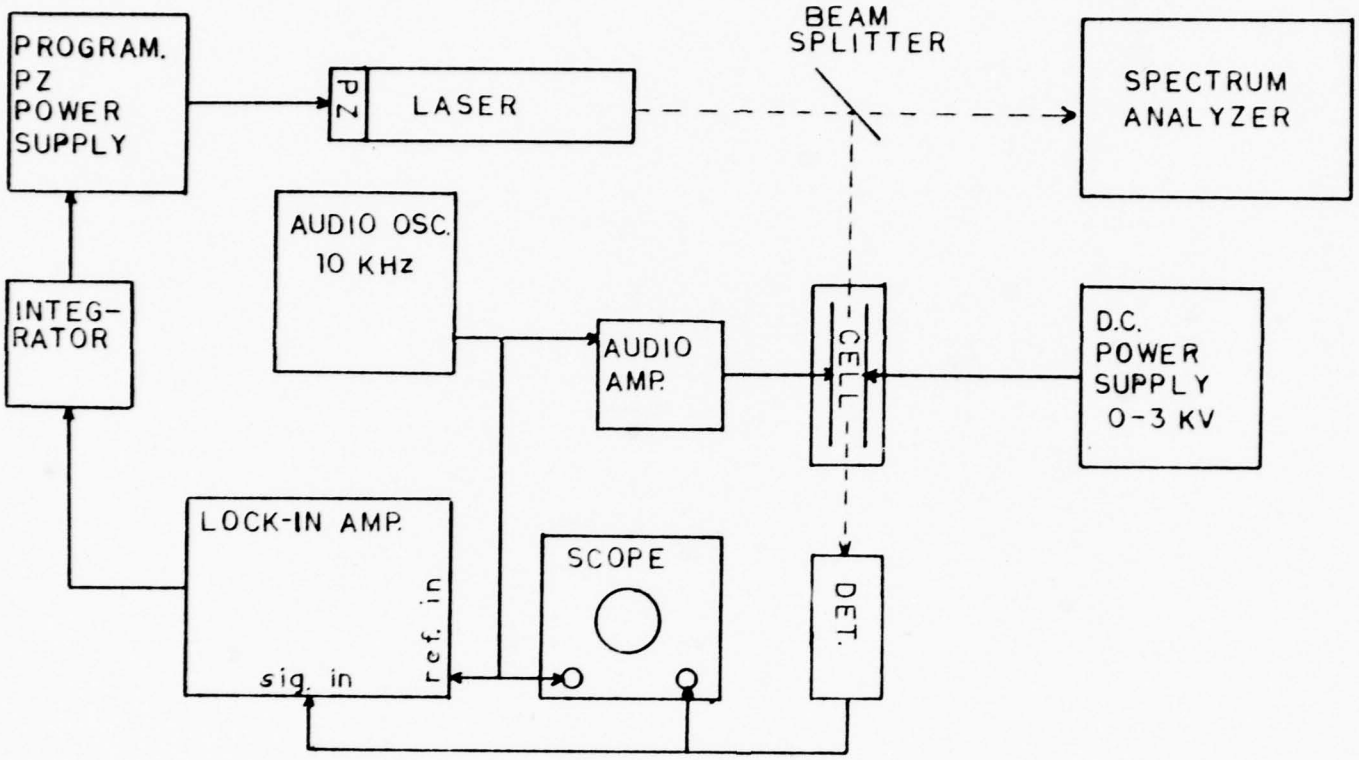


FIGURE 6

supply which in turn drives the piezoelectric-mounted laser cavity mirror. Thus the loop is completed. The exact details of error signal production and the integrator are covered in the experimental part as a result of a computer analysis.

# III. EXPERIMENTAL

The following discussion of experimental procedure and results is specific to the GTE Sylvania Model 941 $CO_2$ Laser whose characteristics are given in Appendix A and to the Stark cell whose characteristics are given in Appendix B. Unless otherwise indicated, wherever the phrases "the laser" or "the Stark cell" appear, it is understood that they refer to the laser and Stark cell described in Appendices A and B.

## A. LINESHAPES

An attempt to determine the lineshapes of the laser transitions experimentally was made by plotting relative intensity and mode as a function of piezoelectric voltage. The experimental arrangement is schematically represented in Fig. 7. The x-axis of the x-y plotter sampled the piezoelectric voltage from terminals 8 and 10 of the PZ power supply through a voltage divider. The PZ power supply is a Kepco Model ABC regulated D.C. supply with a range of 0 to 1500 volts. It was operated in the voltage programmable mode with a positive ground. The programming voltage was a regulated 0 to 25 volt D.C. supply. The battery box and reversing switch were added to obtain the proper biasing for tuning over the full range of the Kepco with a minimum of switching.

# INTENSITY VS PIEZOELECTRIC VOLTAGE EXPERIMENT

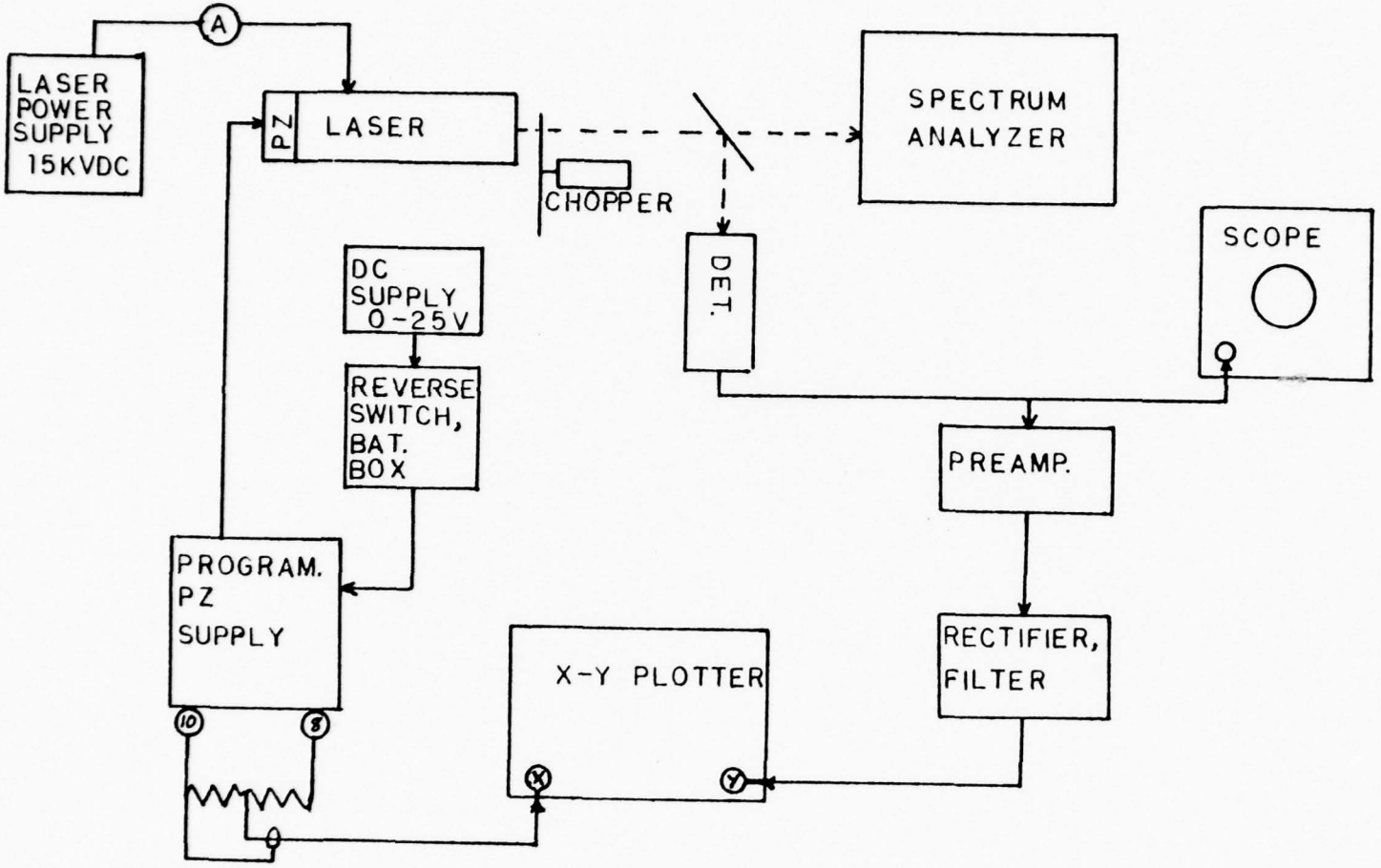


FIGURE 7

The y-axis of the x-y plotter sampled the relative intensity of the chopped laser output via a pyroelectric detector, preamplifier, and a filtered rectifier. The longitudinal mode or vibrational-rotational transition was continuously monitored using an Optical Engineering $CO_2$ Spectrum Analyzer. Frequency could not be monitored due to the lack of precision, but the longitudinal mode could be identified. Typical results are given in Fig. 8 for an increasing PZ voltage and in Fig. 9 for a decreasing PZ voltage.

It is noted that the plots are not identical but a hysteresis effect exists [Ref. 22]. The P(20) line is shifted in the direction of the voltage scan. Various scan rates were tried in order to ascertain that the effect was not due to the response of the instruments. Nine to ten different lines were observed over the tuning range. It is also noted from Figs. 8 and 9 that the series of lines begins to repeat itself after approximately 1.4 kV. Since the resonance condition requires the cavity length be an integer number of half wavelengths, this voltage change corresponds to a length change of half a wavelength and the piezoelectric $\frac{\Delta L}{\Delta V}$ parameter may be estimated as

$$\frac{\Delta L}{\Delta v} \cong \frac{1/2(10.6\ \mu m)}{1.4\ kV} = 3.8\ \mu m/kV \quad . \tag{55}$$

# INTENSITY AND MODE AS FUNCTION OF INCREASING PZ VOLTAGE

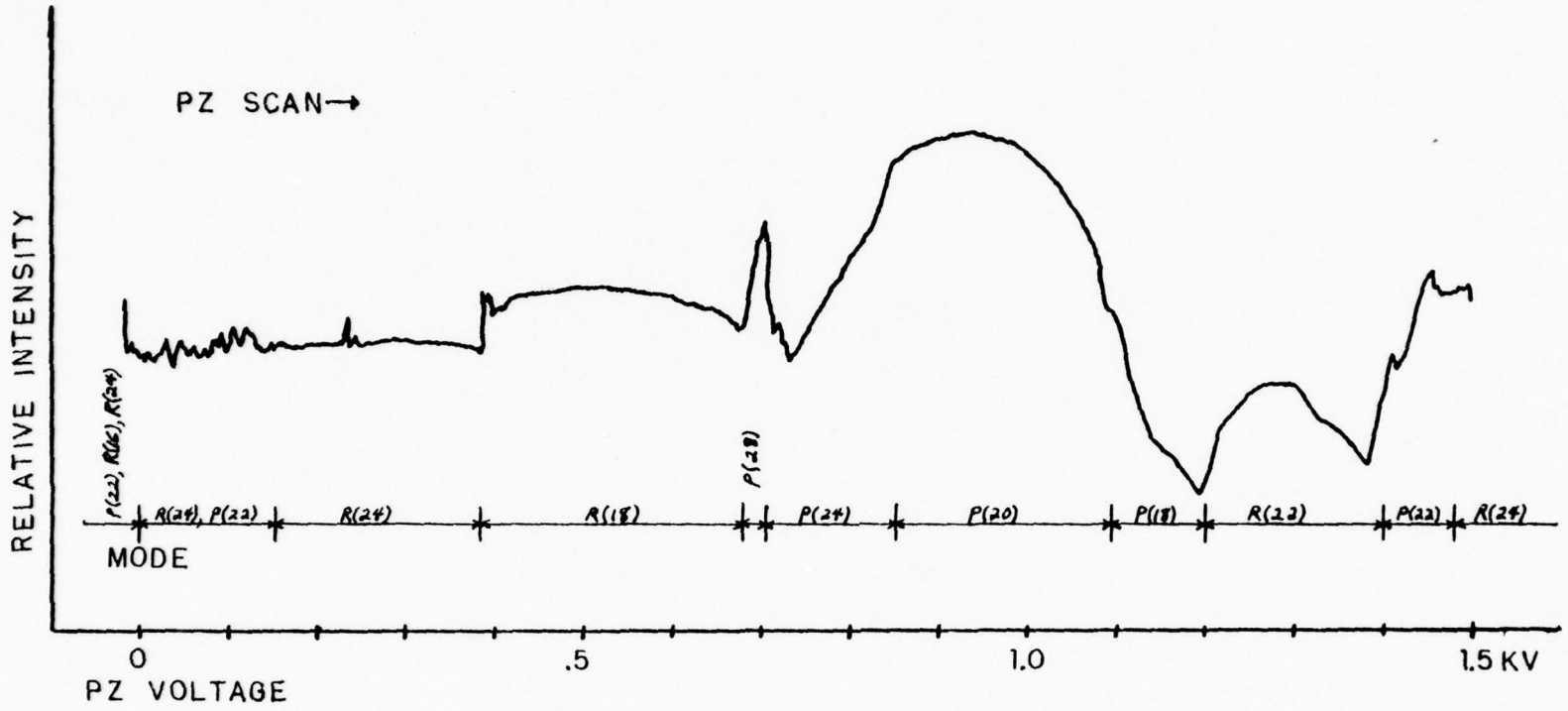


FIGURE 8

# INTENSITY, MODE, AS FUNCTION OF DECREASING PZ VOLTAGE

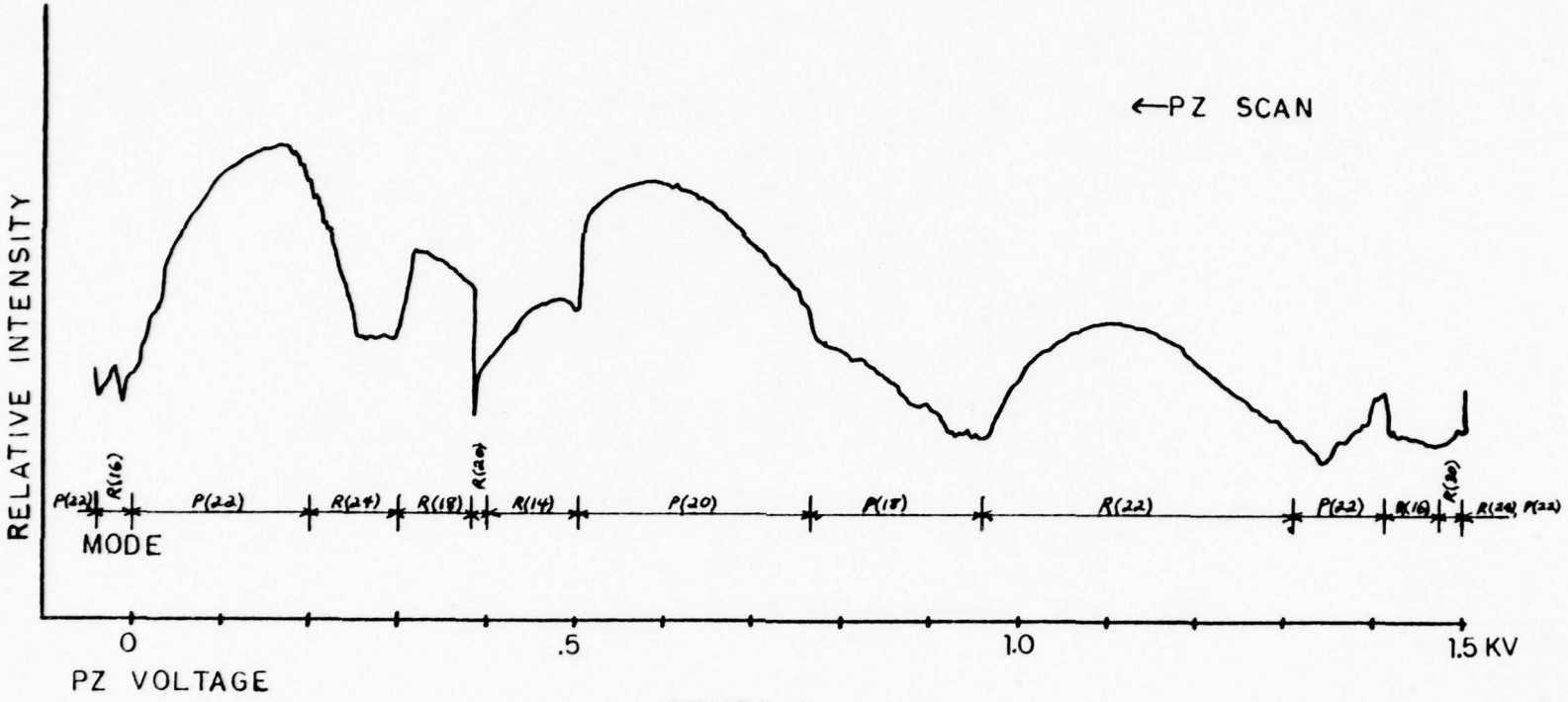


FIGURE 9

It is noted that this value corresponds with the value given by Sylvania. This calculation assumes that the piezoelectric crystal has a linear response to voltage.

From (55) and Figs. 8 and 9 the apparent linewidth of the P(20) transition is estimated to be 55 MHz which is close to the Doppler linewidth given by Sylvania. The cavity linewidth calculated from (38) with $\alpha = 0$ is 19 MHz. The pressure broadened linewidth is 100 MHz and the Doppler linewidth is 50 MHz. The total linewidth using (32) is 112 MHz. Taking the differential of (39) and using 19 MHz for $\Delta\nu_c$, 112 MHz for $\Delta\nu$, and 55 MHz for the change in passive cavity resonance $d\nu_q$, gives a change in oscillation frequency $d\nu$ of 46 MHz, which would be closer to the actual linewidth if the above numbers are correct.

It is concluded that the PZ voltage may be used to estimate the laser oscillation frequency; however, the actual frequency change is only slightly less than the change indicated by the PZ voltage due to the frequency pulling effect. A more precise means of measuring the actual frequency of oscillation would be required to verify (39) and determine the average distributed loss constant $\alpha$. For gross changes in the frequency of oscillation, using the PZ voltage alone will result in insignificant error. To determine small changes such as linewidths a more precise method of measuring frequency is required. It would also be necessary to insert a prism or grating in the cavity to prohibit the neighboring modes from oscillating until the

half power point was reached. From Figs. 8 and 9 it is observed that the half power points are never reached on the P(20) line before the neighboring line begins to oscillate. There is considerable overlapping of the lines. Mode competition is also quite prevalent in a $CO_2$ laser. Thus it is impossible to measure linewidths in the manner attempted above.

B. MODES OF OPERATION

The laser's cavity length is .45 m. This gives from (34) a mode separation of 333 MHz which is considerably larger than the total linewidth of 112 MHz. Consequently the laser should normally oscillate in a single longitudinal mode, which in fact it did. Occasionally two lines were observed to oscillate simultaneously and on one occasion four lines oscillated simultaneously at a coolant temperature of about 18°C; the P(22), R(16) R(24), and R(30) lines. Also a very faint P(14) line of the 9.4 μm band was observed to oscillate simultaneously with P(22) on the 10.4 μm band at 19-20°C coolant temperature out.

The laser utilizes a dielectric flat for the output mirror and a 3 m totally reflecting mirror mounted on a piezoelectric crystal. Using (35) gives a transverse mode separation of 42 MHz, which is less than the total linewidth. From (37) the spot size on the output mirror is 1.9 mm. The laser's bore diameter is 6 mm. Thus from the discussion preceding Eq. (36) the laser is only marginally diffraction limited to the lowest order transverse mode. On

one occasion the $TEM_{10}/TEM_{01}$, the "doughnut" mode, was observed. On another occasion efforts to reproduce this mode yielded only the $TEM_{00}$ mode throughout the full range of the PZ voltages.

## C. INSTABILITIES

Experimentation began with minimization of 60 Hz noise. The voltages on the ground terminals of all 115 VAC receptacles in the lab were measured with respect to a drainpipe ground. One receptacle ground was found to have a 52 mV 120 Hz signal. Its ground strap was isolated from the grounds of the other receptacles in order to minimize the signal on them. The receptacle with the lowest ground signal (5 mV peak to peak at 180 Hz) was used as the source for all measuring instruments and power supplies. Noisy receptacles were used for vacuum equipment, chopper, and heat lamps. Ground loop signals were eliminated only by trial and error.

The laser power supply, the GTE Sylvania model 941P, is unregulated and minimally filtered. It was found to have a one to ten per cent current ripple depending on the discharge current. This was entirely unsuitable for stabilization of the laser as the current ripple showed up in an amplitude modulated laser output. An L-section filter consisting of a .5 μf capacitor and a 45 H choke (which was actually the secondary of a 13 kV transformer) was assembled and connected to the high voltage output at the laser power

supply. Details of the filter are given in Appendix E. The filter reduced the current ripple and consequently the laser output fluctuation by a factor of 50 to approximately .2%. Since a 10% Stark cell modulation was expected, this filter was considered to be suitable for short-term stability purposes. For long-term stability, a well regulated power supply was still required. Plots of laser intensity as a function of excitation current were made using an x-y plotter. The x-axis input was the voltage drop produced by the excitation current across a small resistance element. Typical results are given in Fig. 10. The relative intensity variation is approximately 14%.

The experimental setup for determining the effect of cooling water temperature on the intensity and longitudinal mode is schematically represented in Fig. 11. The coolant output temperature was sampled using a copper-constantan thermocouple referenced to an ice bath. The voltage drop across the thermocouple was measured with a nanovoltmeter on the 3 millivolt scale. The output of the nanovoltmeter drove the x-axis of an x-y plotter. The y-axis sampled the chopped laser intensity via a pyroelectric detector, preamplifier and filtered rectifier. The coolant temperature was slowly increased over a period of about one hour from 7° to 40°C by circulating the coolant through an ice bath and warming the ice bath with a heating element. The longitudinal mode was continuously monitored using a spectrum analyzer. Mode changes were noted and recorded on the plot

# INTENSITY & MODE AS A FUNCTION OF TUBE CURRENT

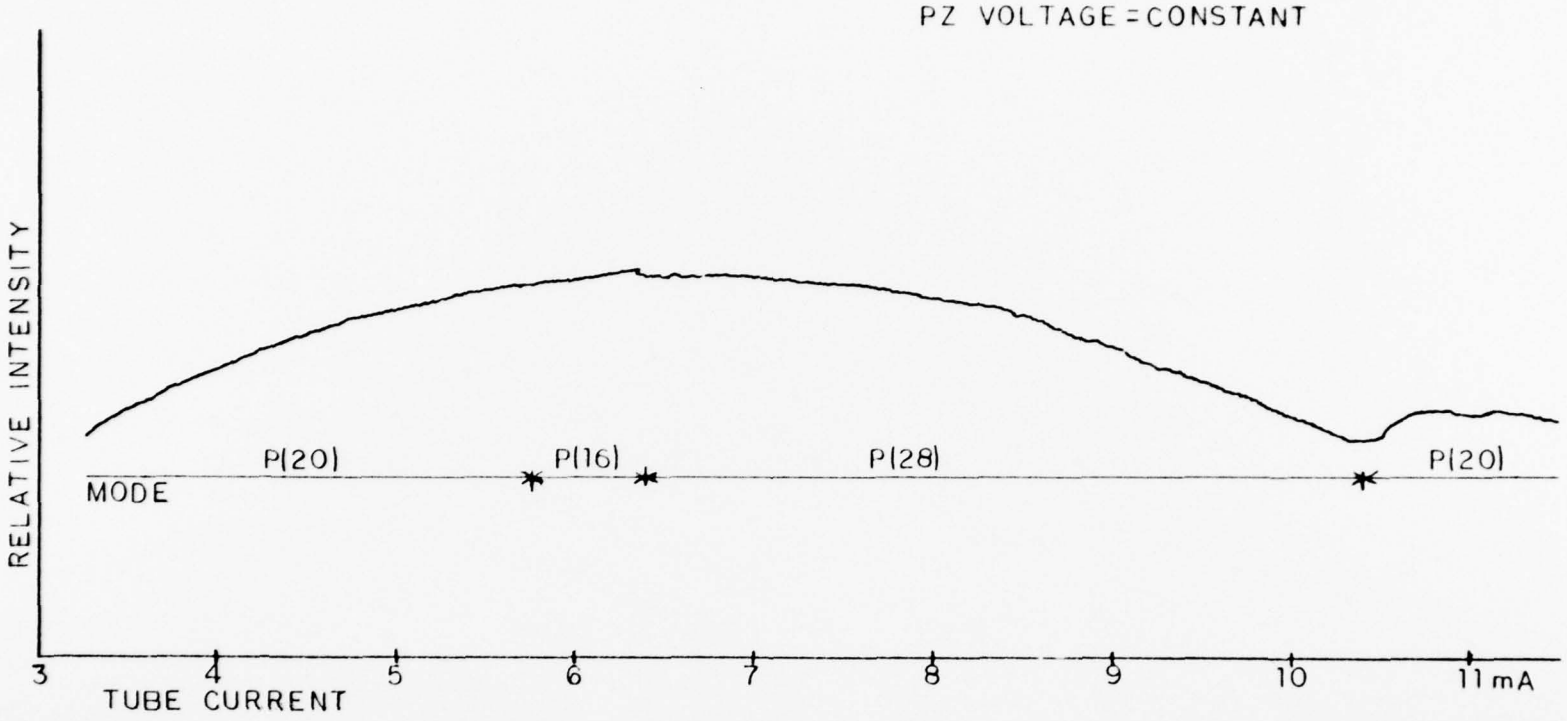


FIGURE 10

# INTENSITY VS TEMPERATURE EXPERIMENT

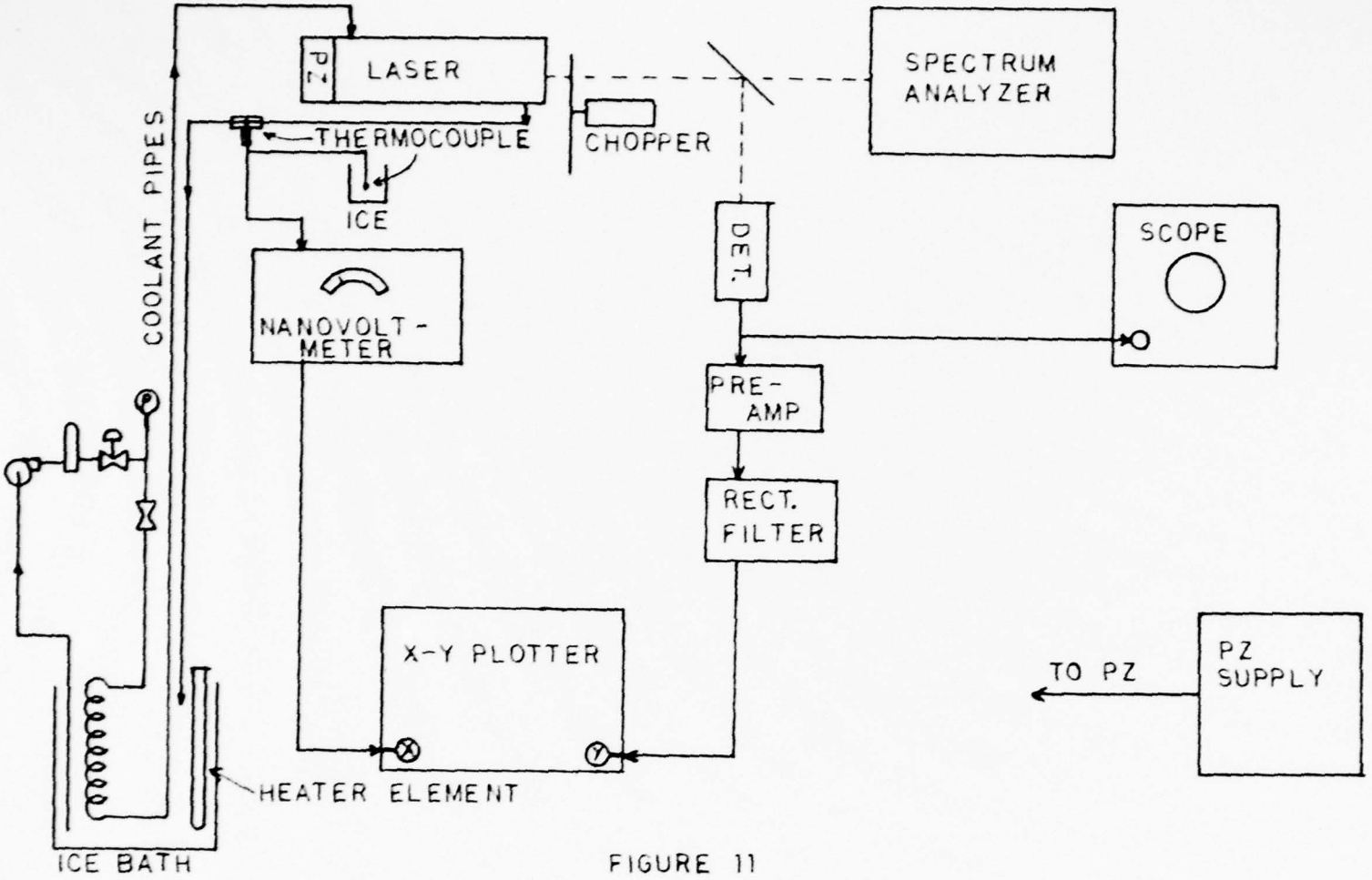


FIGURE 11

after each run. A table of temperature as a function of thermocouple voltage is given in Appendix F.

Figure 12 is a plot with the PZ voltage held constant. Note that the series of lines from P(18) to R(22) is repeated in identical order; however, there is little similarity to the intensity profiles. The P(18) line is repeated twice over a temperature range of 8.8 to 37.9°C. Since the resonance condition requires the cavity length to be exactly an integer number of half wavelengths of the oscillation frequency, this temperature range corresponds to a thermal expansion of two half wavelengths or one wavelength of the P(18) transition. Thus the thermal coefficient may be determined from Eqs. (45) and (46) as

$$\alpha = \frac{1}{L}\frac{dL}{dT} = \frac{1}{.45}\frac{(10.57 \times 10^{-6})}{29.1°C} = 8 \times 10^{-7}/C° \ . \qquad (56)$$

Note that this calculation assumes that a temperature change in coolant out corresponds to an equal temperature change in the laser tube wall. See Appendix G for proof of this.

The plot shows an overall decrease in intensity output with increasing temperature, by a factor of about two in a temperature range of 33C°. It is also obvious that the P(20) transition is the strongest in the group. P(22), R(16) and R(24) form a competing trio. Mode competition is almost always present between these lines. All three or pairs of these lines are often observed oscillating simultaneously.

# INTENSITY & MODE AS FUNCTION OF INCREASING TEMPERATURE

(COOLING WATER OUT)

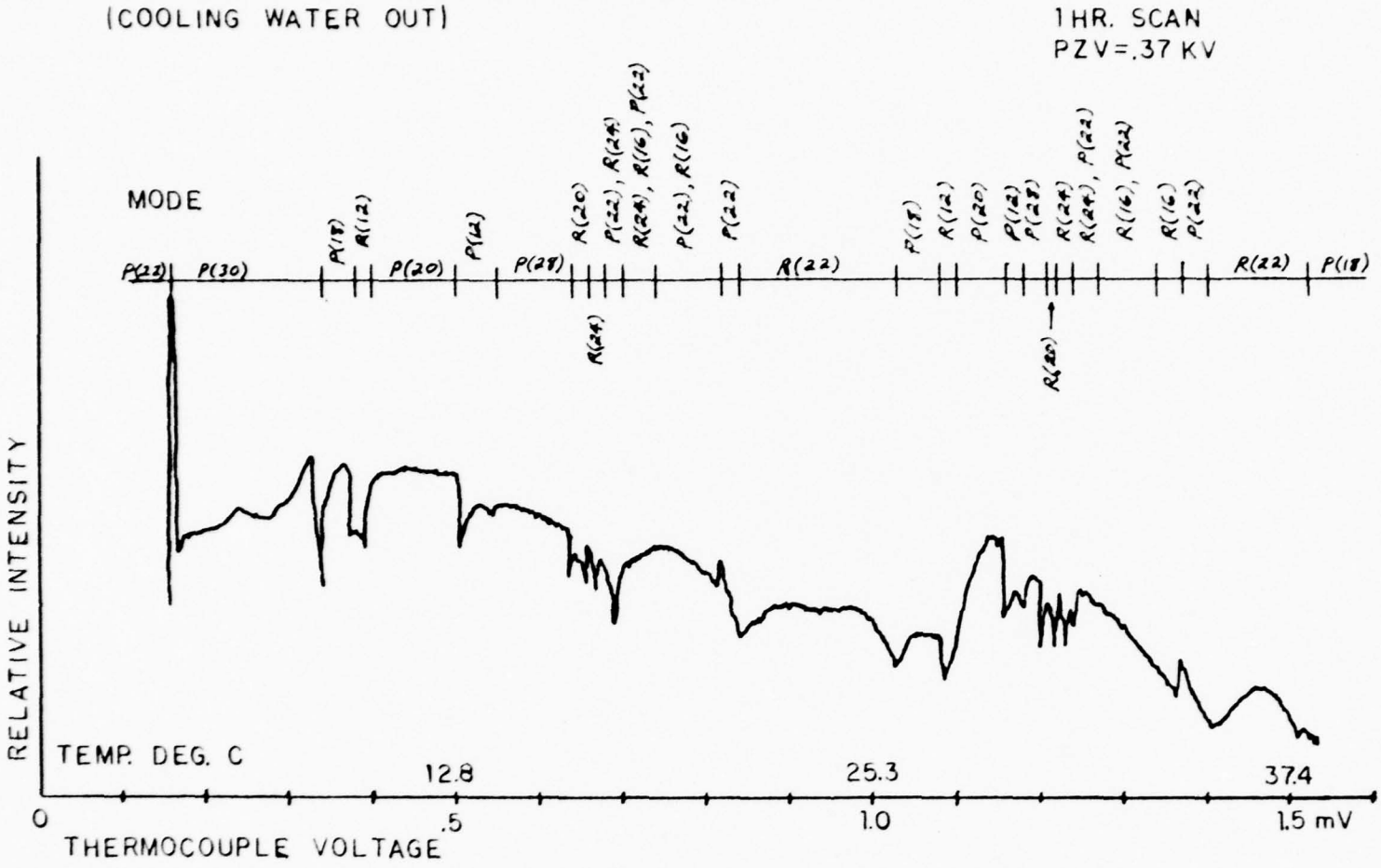


FIGURE 12

It would therefore be wise to avoid stabilizing on any one of these three lines.

Figure 13 shows the maximum intensity of the P(20) line as a function of temperature. The intensity decreases almost linearly with increasing temperature. The region between 7 to 27°c shows mode competition. It is also noted from Fig. 13 that as temperature increases or the cavity expands, the PZ voltage had to be increased in order to maintain the P(20) line. It follows that an increasing PZ voltage corresponds to a decreasing cavity length and the sign on the $\frac{\Delta L}{\Delta V}$ parameter given by (55) should be negative.

An experiment was performed to determine the effect of coolant flow rate fluctuations on the laser cavity. The flow rate was adjusted within the limits set by Sylvania from 11 ml/s to 30 ml/s at a constant temperature input. The temperature output changed as expected from 23.8 to 22.8°C. Using (56) this one-degree temperature change corresponds to a length change of .36 μm. In this experiment the PZ voltage was adjusted to maintain maximum intensity on the P(20) line, and was adjusted from .42 kV to .24 kV. Using (55) this voltage change corresponds to a length change of .68 μm which is almost twice the length change accountable for temperature. It follows that a flow rate fluctuation of 19 ml/s results in a length fluctuation of approximately .32 μm. From (45) this corresponds to a frequency fluctuation of 22.6 MHz.

# INTENSITY & PZ VOLTAGE OF P(20) MODE

AS FUNCTION OF INCREASING TEMPERATURE OF
COOLING WATER OUT

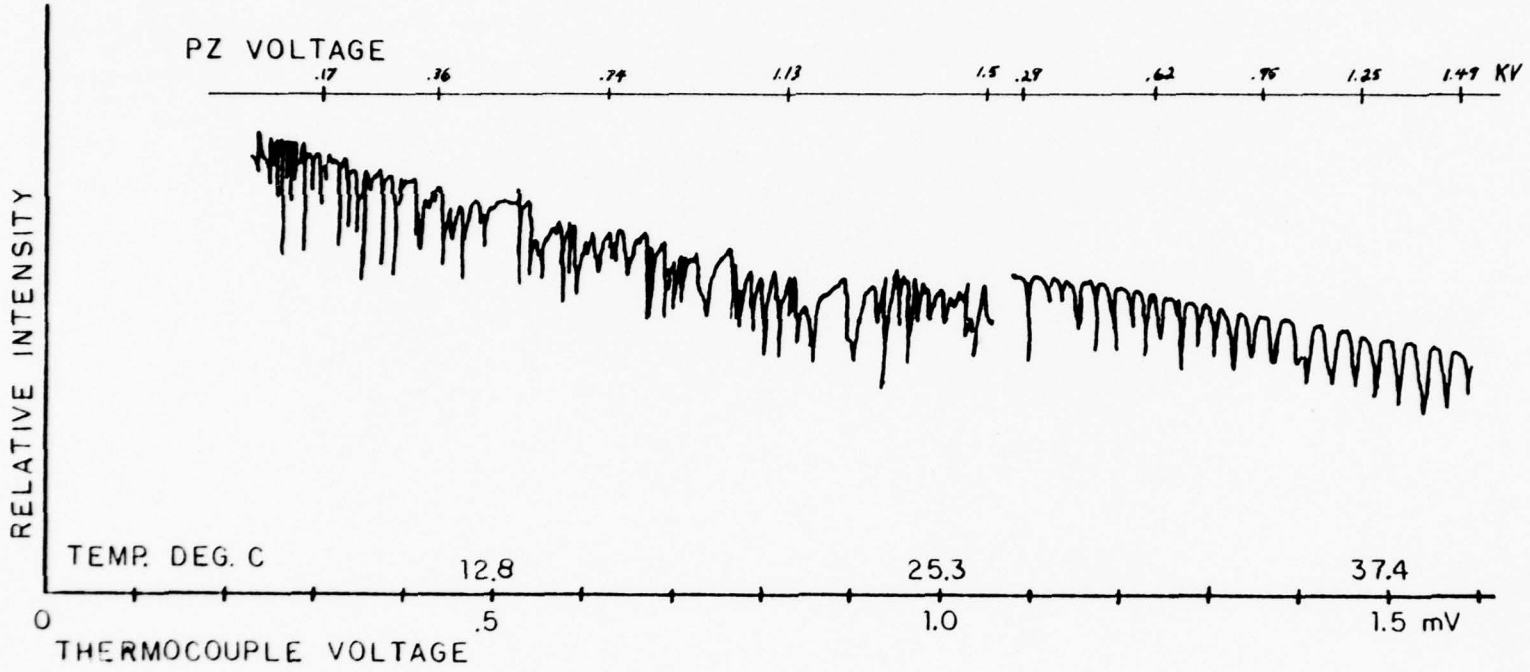


FIGURE 13

It is concluded from these experiments that temperature and flow rate fluctuations are the dominant causes of instability in the laser. Current fluctuations can be easily remedied with a filtered current regulated power supply. If a circulation pump is used for cooling, the system should be well designed to minimize pressure and flow rate fluctuations. Experiments could not be carried out to determine the effects of acoustic vibration due to a lack of a method for precisely measuring small, rapid fluctuations in frequency.

## D. ERROR SIGNAL ANALYSIS FOR A PYROELECTRIC DETECTOR

Drawing an analogy with electrical communication theory it is observed that the stabilization technique is similar to frequency demodulation. The input laser beam is frequency modulated with noise. It is desired to have some sort of frequency discriminator which will sense the shift in frequency and produce an output voltage linearly proportional to the shift. This is precisely what FM demodulation accomplishes [Ref. 23]. The stabilization servo loop is completed when the demodulation information is fed back to the laser to make corrections to minimize the noise modulation.

The exact details of producing an error signal were not clear in the literature. Questions which needed to be resolved were: is the error signal produced by slope or peak detection, how does dithering produce an error signal,

is the composite detector signal or one of its harmonics monitored, and which harmonic should be monitored?

In order to search for a suitable error signal we begin by assuming the transmitted intensity of the cell of length L is of the form

$$I(\nu) = I_o(\nu) \exp [-\gamma(\nu)L] \tag{57}$$

where $I_o(\nu)$ is the input intensity, $\gamma(\nu)$ is the absorption coefficient, and $I(\nu)$ is the output intensity as a function of frequency. It is assumed that $I_o(\nu)$ is a narrow spectral laser line of half width much less than the cell absorption linewidth. Thus $I_o(\nu)$ may be approximated by a Dirac delta function, $\delta(x)$. If the frequency of the laser is allowed to vary randomly with time over the linewidth of the absorption cell, and the linewidth of the absorption cell is assumed to be much less than the laser's molecular linewidth so that the laser intensity does not change appreciably over the cell linewidth, then (57) becomes

$$I_\nu(t) = \int_o^\infty I_o \delta(x(t) - \nu) e^{-\gamma(\nu)L} \, d\nu = I_o \exp [-\gamma(x(t))L] \tag{58}$$

where $x(t)$ is a random variable of time and takes on values of frequency within the cell's absorption linewidth. The subscript $\nu$ on I denotes that I is approximated by a delta function, i.e., all the intensity is concentrated at a single frequency.

Equation (58) shows that the frequency modulation x(t) has been converted to an intensity modulation I(t) by simply passing the laser beam through a selective absorber or optical notch filter. It is possible to derive an error signal from I(t) by stabilizing about a point on the slope of $\gamma(\nu)$. This is called slope detection, analogous to slope detection in radio FM demodulation. Two problems arise with slope detection; spurious intensity variations in the laser beam also show up in the error signal and the range of the linear slope is quite small [Ref. 23]. To partially overcome these problems, it is desirable to obtain an error signal which is similar to the frequency to voltage characteristic of a common FM balanced discriminator, where the voltage goes to zero at the center frequency, increases positively on one side of the center frequency, and increases negatively on the other side.

Consider the effect of modulating the center frequency of the absorption cell with an audio signal of frequency $\omega$ according to (53), and using phase-sensitive detection in order to determine zero time. This is schematically represented in Fig. 14. The modulating signal will dither the absorption profile about $\nu_o$ at frequency $\omega$. The amplitude of the dither is $\Delta\nu'$. It is assumed that the dither is much more rapid than the random variation of the laser frequency $\nu$. As will become more apparent later the reason for the assumption is to detect x(t). Only fluctuations

# DITHER MECHANISM

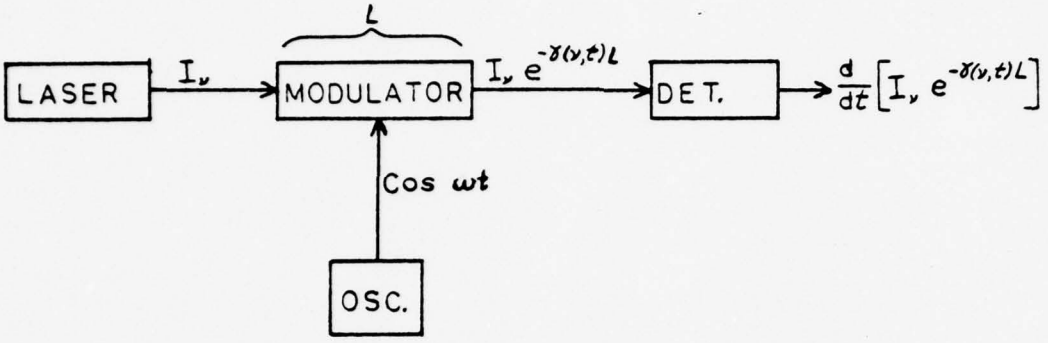


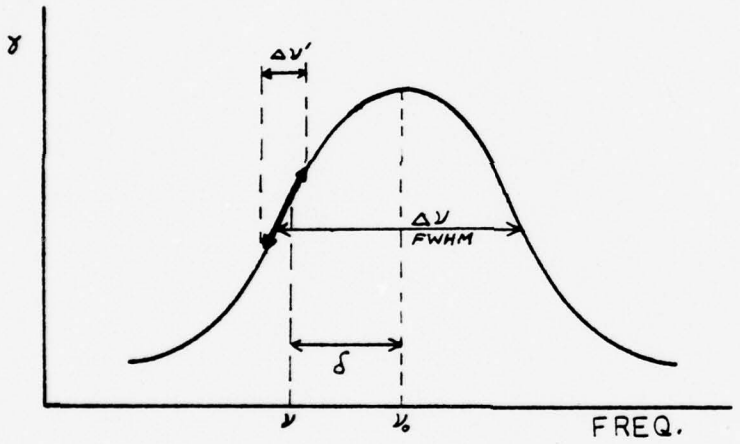


$\Delta\nu$ = FULL WIDTH AT HALF MAXIMUM

$\Delta\nu'$ = AMPLITUDE OF DITHER

$\nu$ = LASER FREQUENCY

$\nu_0$ = AVERAGE CENTER ABSORPTION FREQUENCY

FIGURE 14

slower than $\omega$ can be detected. The end result of the analysis to follow is that x(t) amplitude modulates a "carrier frequency" $\omega$. It would be desirable to make $\omega$ extremely large in order to detect as much noise as possible. However, as Claspy and Pao [Ref. 18] show, the upper limit for $\omega$ is the homogeneous linewidth. This is reasonable if one considers that from (18) the linewidth was derived from the decay time. It is now observed that the decay time is also the absorption time. Thus if a molecule does not remain in resonance with the passing radiation for the duration of the absorption time, the molecule will not absorb. In other words, the Stark cell is bandwidth limited by the homogeneous linewidth.

The detector used in this part of the analysis has an output voltage proportional to the time rate of change of the incident intensity. An example of such a detector is a pyroelectric. This time-differentiating detector will be referred to as "detector A" in this analysis.

The absorption coefficient of the cell is assumed to have a Lorentzian shape from (19).

$$\gamma(\nu) = Sg(\nu) = \frac{S\Delta\nu}{2\pi\left[\left(\frac{\Delta\nu}{2}\right)^2 + (\nu - \nu_o)^2\right]} \tag{59}$$

where S is the line strength and is a constant. The absorption coefficient is given a time dependence by oscillating the center resonant frequency according to (53).

$$\gamma(\nu,t) = \frac{S\Delta\nu}{2\pi\left[\left(\frac{\Delta\nu}{2}\right)^2 + (\nu - \nu_o - \Delta\nu' \cos \omega t)^2\right]} \tag{60}$$

The difference in frequency between the laser beam and the average center resonant frequency $\nu_o$ is defined as $\delta = \nu - \nu_o$ , where the symbol used is not to be confused with the Dirac delta used earlier. Equation (60) then becomes

$$\gamma(\nu,t) = \frac{S\Delta\nu}{2\pi\left[\left(\frac{\Delta\nu}{2}\right)^2 + (\delta - \Delta\nu' \cos \omega t)^2\right]} \tag{61}$$

Substituting (61) into (58) the intensity out as a function of time is given by

$$I(t) = I_o \exp\left[-\frac{S\Delta\nu L}{2\pi\left[\left(\frac{\Delta\nu}{2}\right)^2 + (\delta - \Delta\nu' \cos \omega t)^2\right]}\right] \tag{62}$$

Detector A output as a function of time is a voltage proportional to

$$f(t) = \frac{dI(t)}{dt} = -I_o SL \frac{dg(\nu,t)}{dt} \exp\{-SL\, g(\nu,t)\} \tag{63}$$

As was assumed earlier the oscillation frequency is much greater than the random variation of the laser frequency $\nu$.

Thus $\delta$ is approximately constant and the derivative with respect to time of (62) may be taken holding it as such. Taking the derivative of (59), expanding all squared terms and using common trigonometric identities yields

$$S\frac{dg(\nu,t)}{dt} = \frac{-S\Delta\nu\Delta\nu'\omega(\delta \sin \omega t - \frac{\Delta\nu}{2} \sin 2\omega t)}{\pi[A+B\cdot\cos \omega t + C\cdot\cos 2\omega t + D\cdot\cos 3\omega t + E\cdot\cos 4\omega t]}$$

where

$$A = \delta^4 + 3\delta^2(\Delta\nu')^2 + \frac{3}{8}(\Delta\nu')^4 + (\frac{\Delta\nu}{2})^2\, 2\delta^2 + (\frac{\Delta\nu}{2})^2(\Delta\nu')^2 + (\frac{\Delta\nu}{2})^4$$

$$B = -4\delta^3\Delta\nu' - 3\delta(\Delta\nu')^3 - 4\delta\Delta\nu'(\frac{\Delta\nu}{2})^2$$

$$C = 3\delta^2(\Delta\nu')^2 + \frac{1}{2}(\Delta\nu')^4 + (\Delta\nu')^2(\frac{\Delta\nu}{2})^2 \qquad (64)$$

$$D = -\delta(\Delta\nu')^3$$

$$E = \frac{1}{8}(\Delta\nu')^4$$

Equation (63) can be simplified if $\gamma(\nu,t)L << 1$. The exponential then is approximately one and f(t) is proportional to (64). Note that S could be determined experimentally by applying a D.C. field and measuring the transmitted intensity when $\nu = \nu_o$ and when $|\nu - \nu_o| >> \Delta\nu$.

Equation (64) was plotted on a HP 9810A calculator for various values of $\delta$ and $\Delta\nu'$. The full width at half maximum $\Delta\nu$ and the period of the fundamental oscillation T were arbitrarily set to one in the program; thus $\omega$ the

fundamental frequency is $2\pi$. $\delta$ is varied between -1.0 and 1.0 and $\Delta\nu'$ between 0.1 and 1.0. The results are plotted in Figs. 15, 16, 17, and 18. Figure 15 is for $\delta = 0$ and $\Delta\nu' = .1$ and .7. Note the frequency is twice the fundamental. This would be expected for a laser line oscillating symmetrically about the peak of a transfer characteristic. From (64) it is also noted that when $\delta = 0$ no fundamental or first harmonic exists. Figure 15 also reveals the nonlinearity produced by overdriving with a large $\Delta\nu'$. Though the output signal is greater, higher order harmonics are obviously present, producing a distorted sin $2\omega t$.

Figure 16 is for $\delta = .2$ and $\Delta\nu' = .1$ and .7. It is obvious that some first harmonic is present. It is noted that when $\Delta\nu' > \delta$ the dither carries the line to both sides of the $\gamma(\nu)$ peak, thus producing a large amount of second harmonic but because the dither is unsymmetrical about the peak of $\gamma(\nu)$ a small amount of first harmonic is generated. When $\delta > \Delta\nu'$ second harmonic is virtually nonexistent.

Figure 17 is for $\delta = .5$ and $\Delta\nu' = .1$ and .7. This is the region of slope detection. A considerable amount of first harmonic is obviously present. Very little second harmonic is present even when $\Delta\nu'$ is greater than $\delta$. Figure 18 shows a 180° phase shift in going from a positive $\delta$ to a negative $\delta$.

It is concluded from these four plots that the basic requirements for generating an error signal are present; the

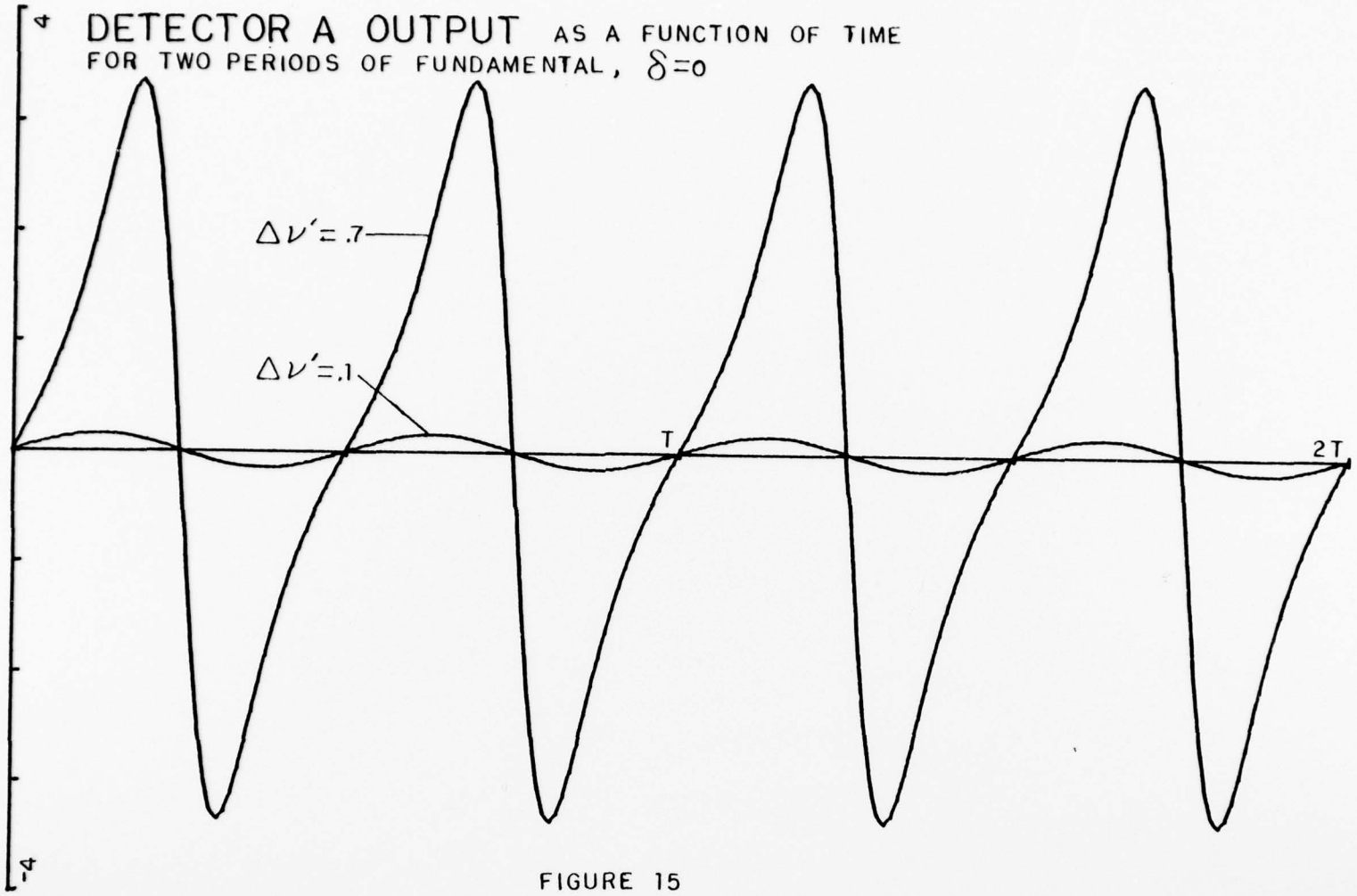
DETECTOR A OUTPUT AS A FUNCTION OF TIME
FOR TWO PERIODS OF FUNDAMENTAL, δ=0
4
-4
Δν'=.7
Δν'=.1
T
2T

FIGURE 15

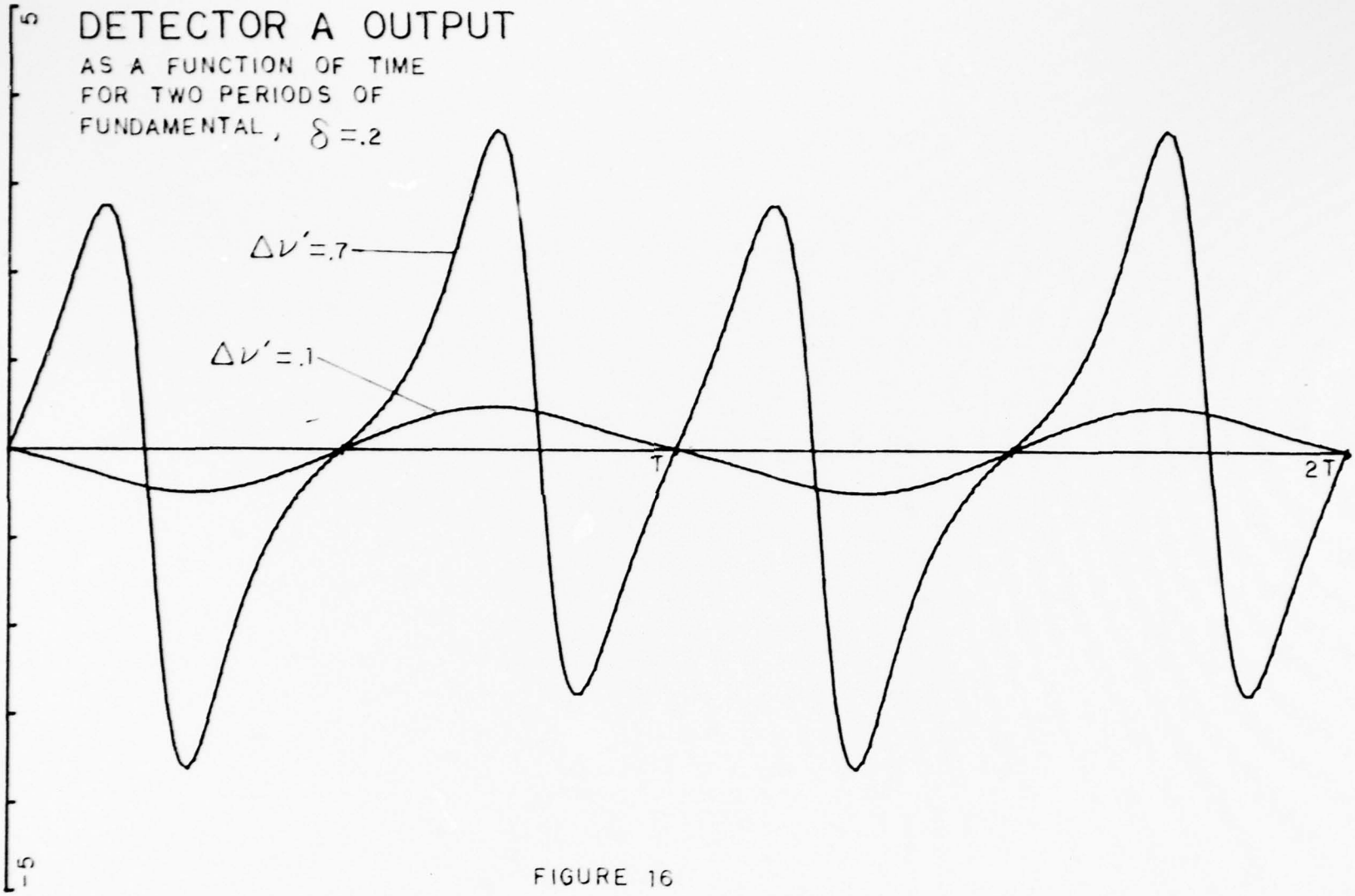
DETECTOR A OUTPUT
AS A FUNCTION OF TIME
FOR TWO PERIODS OF
FUNDAMENTAL, δ =.2
Δν'=.7
Δν'=.1
5
-5
T
2T

FIGURE 16

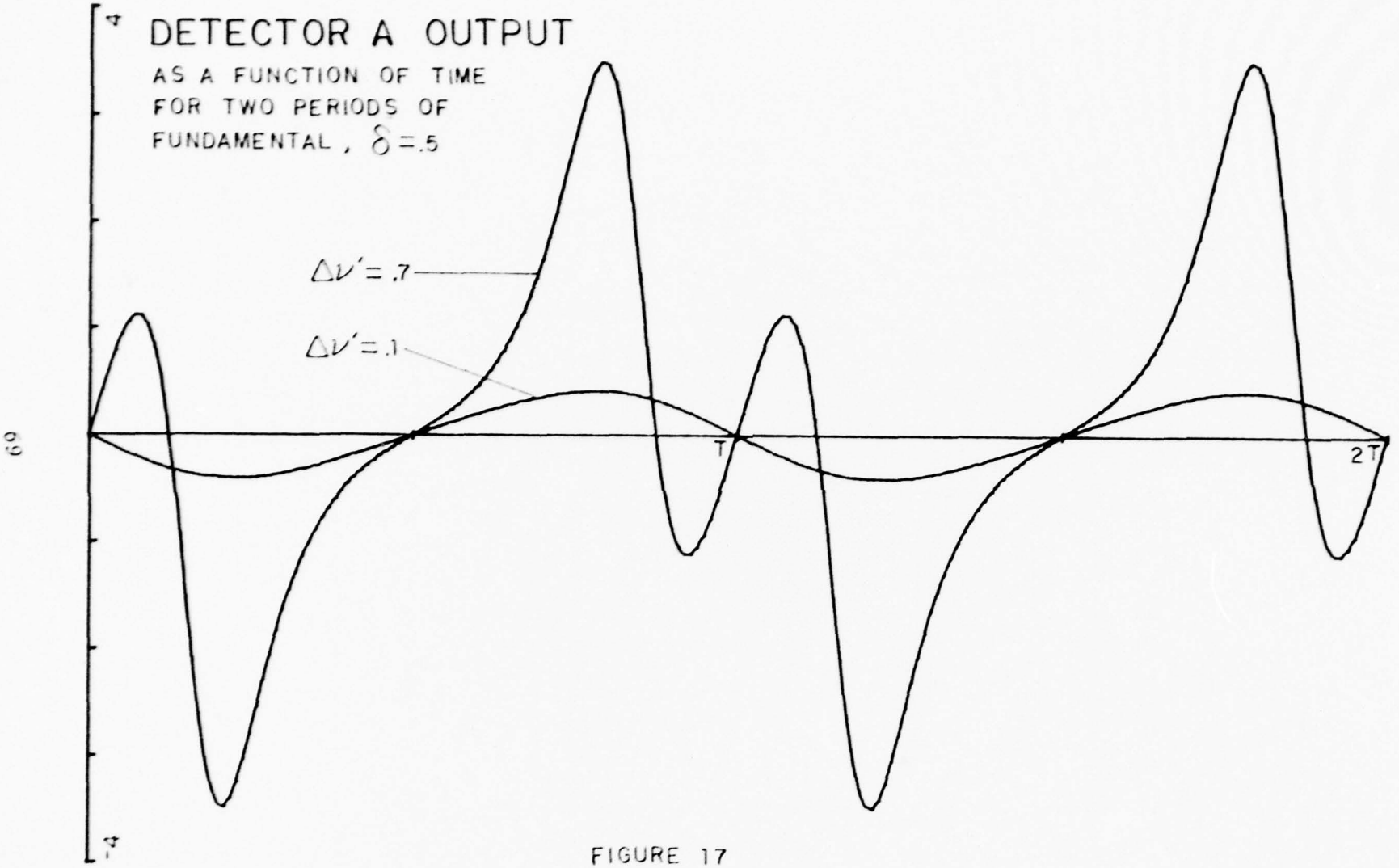
DETECTOR A OUTPUT
AS A FUNCTION OF TIME
FOR TWO PERIODS OF
FUNDAMENTAL, δ=.5
Δν'=.7
Δν'=.1
T
2T

FIGURE 17

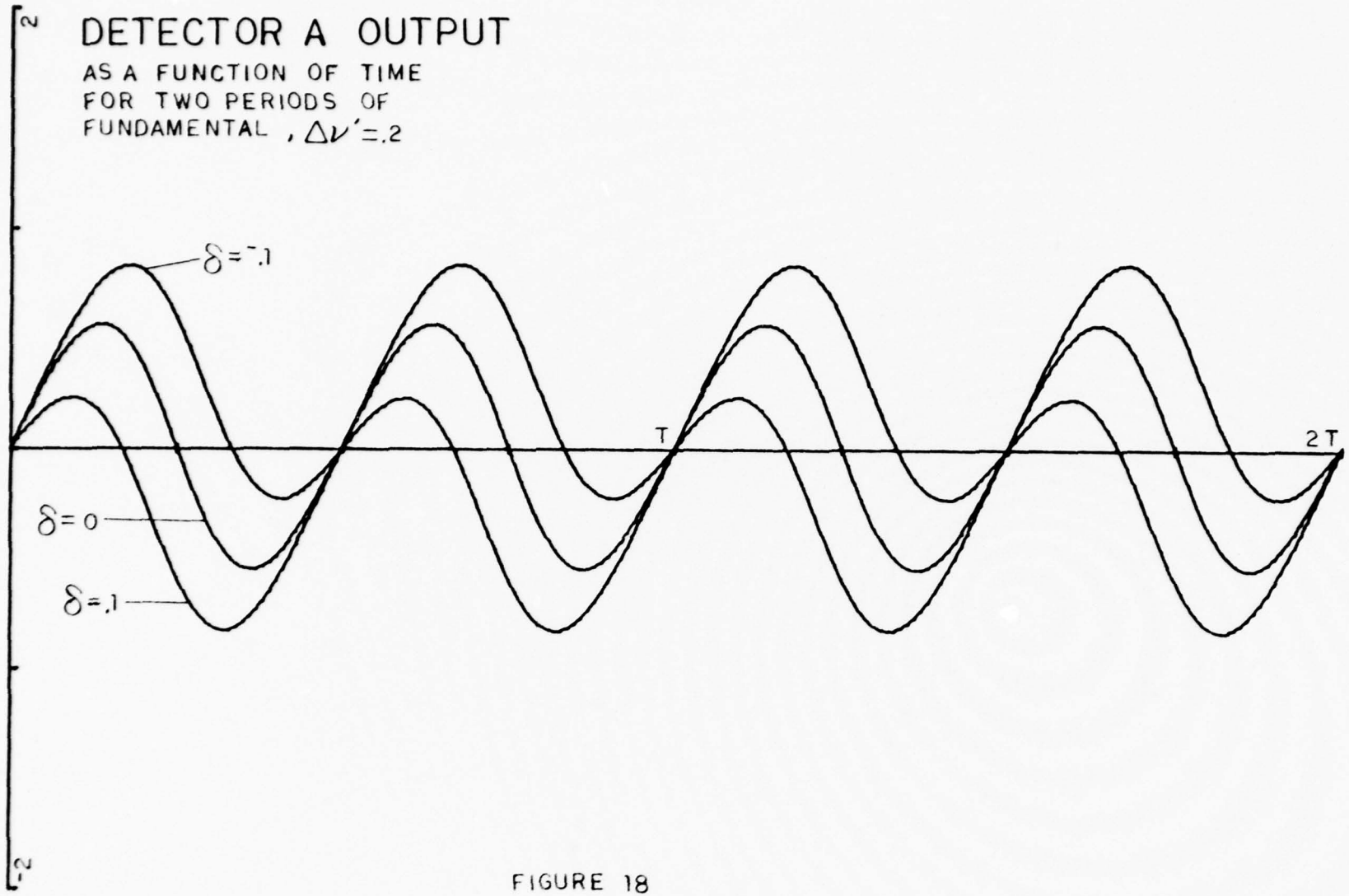
DETECTOR A OUTPUT
AS A FUNCTION OF TIME
FOR TWO PERIODS OF
FUNDAMENTAL , $\Delta\nu' = .2$
2
-2
$\delta = -.1$
$\delta = 0$
$\delta = .1$
T
2T

FIGURE 18

amplitude of the signal indicates the magnitude of $\delta$ and the phase of the signal indicates the sign of $\delta$. Thus the distance of the laser frequency from the reference $\nu_o$ is known and the direction from $\nu_o$ is known. It is still desired, however, to obtain the typical FM frequency discriminant and to determine which harmonic to monitor or if the composite signal should be monitored.

It is revealing to decompose the signal of (64) into all the harmonics which make up the signal and examine each harmonic singly. Any periodic signal of fundamental period T which is bounded and real may be expanded into a Fourier series according to

$$f(t) = \frac{a_o}{2} + \sum_{n=1}^{\infty} \left(a_n \cos \frac{n2\pi t}{T} + b_n \sin \frac{n2\pi t}{T}\right)$$

where

$$a_n = \frac{2}{T} \int_o^T f(t) \cos \frac{n2\pi t}{T} \, dt \, , \; n = 0, 1, 2 \ldots$$

$$b_n = \frac{2}{T} \int_o^T f(t) \sin \frac{n2\pi t}{T} \, dt \, , \; n = 1, 2, \ldots \qquad (65)$$

For the complex signal given by (64) the integration cannot be performed analytically; however, it can be performed numerically on a computer. It is known that for an odd function of t, i.e., $f(-t) = -f(t)$, which is what the

plots show (64) to be, all the $a_n$'s will integrate to zero over one period. Thus only the $b_n$'s need be calculated. For a fundamental period of T = 1, Eq. (65) reduces to solving the problem

$$f(t) = \sum_{n=1}^{\infty} b_n \sin (n2\pi t)$$

$$b_n = 2 \int_0^1 f(t) \sin (n2\pi t)\, dt \quad n = 1, 2, \ldots \qquad (66)$$

for f(t) proportional to (64).

A program for the HP 9810 was written to do the numerical integration of (66) up to n = 10 for various values of $\delta$ and $\Delta\nu'$ and print the results. It was concluded that the Fourier coefficients $b_n$ for harmonics greater than n = 3 were too small to be of any value in stabilization. A program was then written to calculate the Fourier coefficient $b_n$ for a particular n preset into the calculator for 200 different values of $\delta$ from -1.0 to 1.0 and plot the results. As before $\Delta\nu$ and $T_o$ were arbitrarily set to one. $\Delta\nu'$ and $\delta$ have the same units as $\Delta\nu$ and are to be viewed as a fraction of the linewidth $\Delta\nu$. $\Delta\nu$ may be scaled up to any desired linewidth; $\delta$ and $\Delta\nu'$ are then scaled up with the same scaling factor. This program is given in Appendix D.

Plots of the first three Fourier b coefficients of (64) as a function of $\delta$, with S = 1, are shown in Figs. 19,

20, 21, and 22. Figures 19 and 20 are the typical shape of an FM discriminant. These plots represent the relative magnitude of the D.C. error signal produced by a lock-in amplifier when only a single harmonic is phase sensitively detected with the oscillator signal to the cell as the reference. Other harmonics could be filtered out using a narrow band pass filter. Figures 19 and 20 show that the first harmonic should be monitored. Note the linear region near $\delta = 0$. When the laser frequency is at $\nu_o$ the error signal is zero. As the laser frequency drifts to the right of $\nu_o$ for a positive $\delta$ the error signal increases linear and negative. A drift to the left of $\nu_o$ would give a positive error signal. This is called peak detection as the laser frequency is stabilized about the peak of the absorption profile.

Figure 20 shows that a large dither amplitude produces a suitable error signal. Note that the peaks are further away from center than for a small dither amplitude. Figure 21 shows that the second harmonic is unsuitable for producing an error signal. However, it might be used in conjunction with the first harmonic for making a gross correction to the laser cavity. Note that if the laser frequency drifts beyond the peaks of the first harmonic signal, the second harmonic goes negative indicating that the range of stability has been exceeded and a gross correction to the laser cavity in the direction indicated by the sign of the first harmonic is required in order to

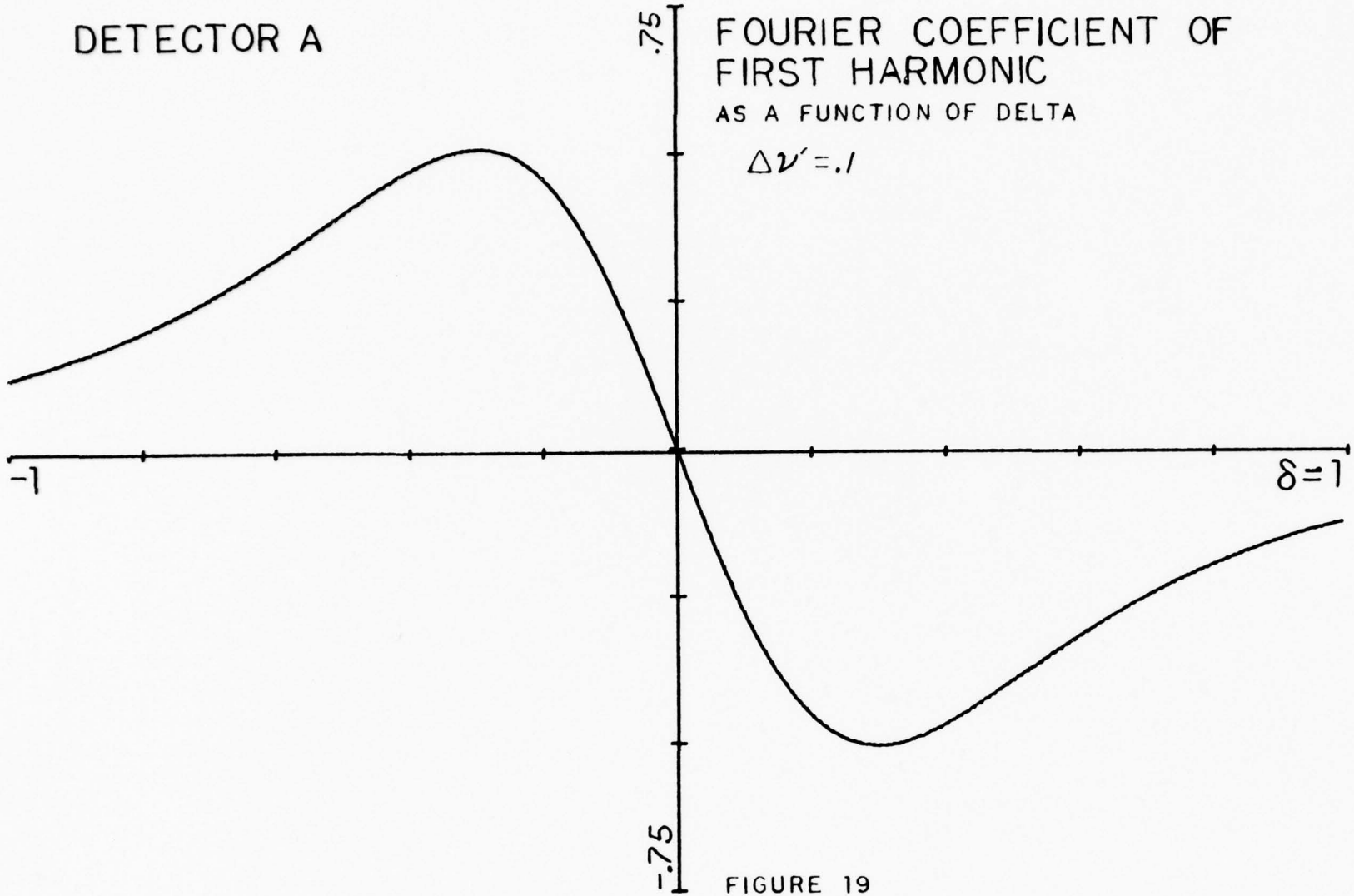
DETECTOR A
.75
FOURIER COEFFICIENT OF
FIRST HARMONIC
AS A FUNCTION OF DELTA
$\Delta\nu' = .1$
-1
$\delta = 1$
-.75

FIGURE 19

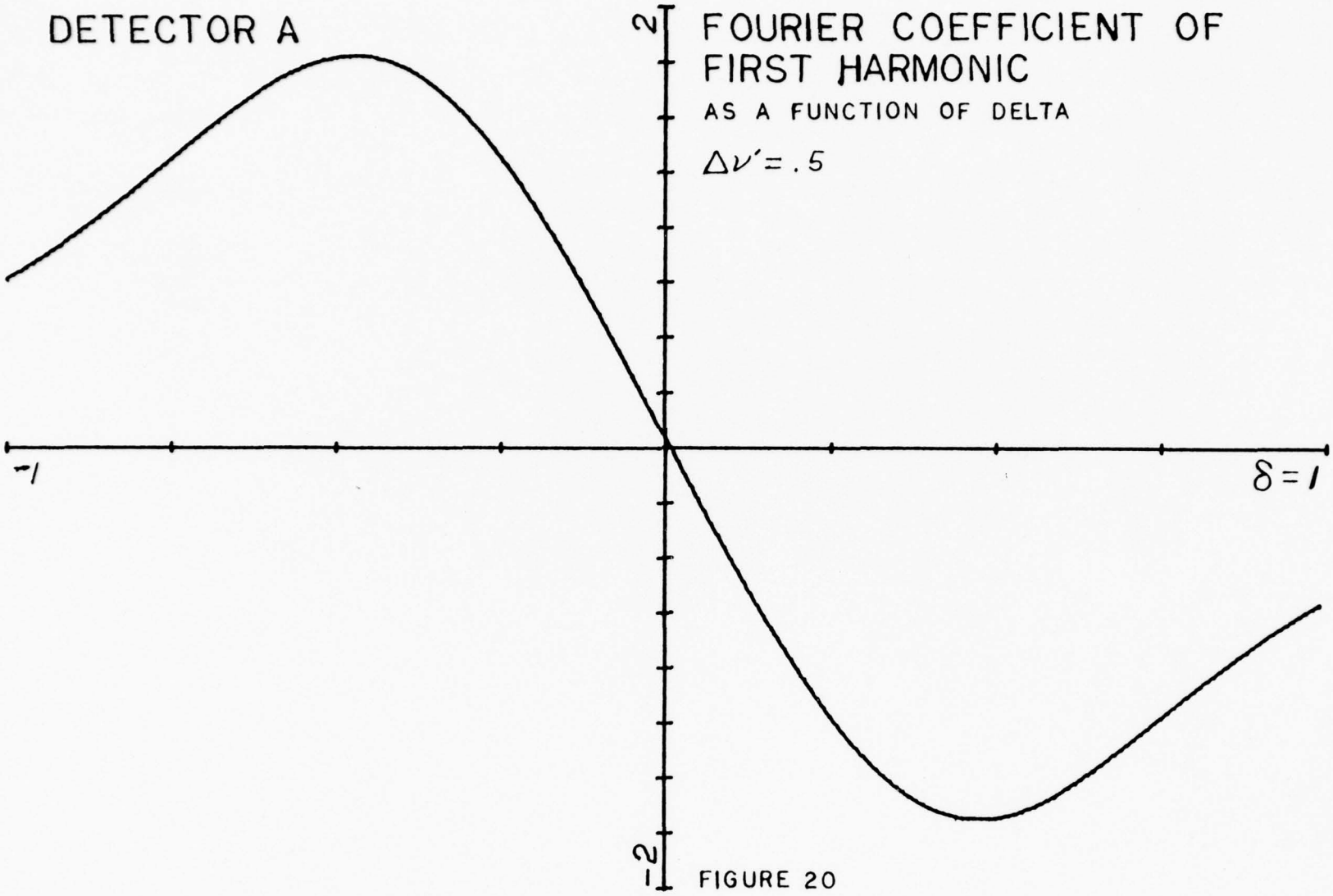
DETECTOR A
FOURIER COEFFICIENT OF FIRST HARMONIC
AS A FUNCTION OF DELTA
$\Delta\nu' = .5$
2
-2
-1
$\delta = 1$

FIGURE 20

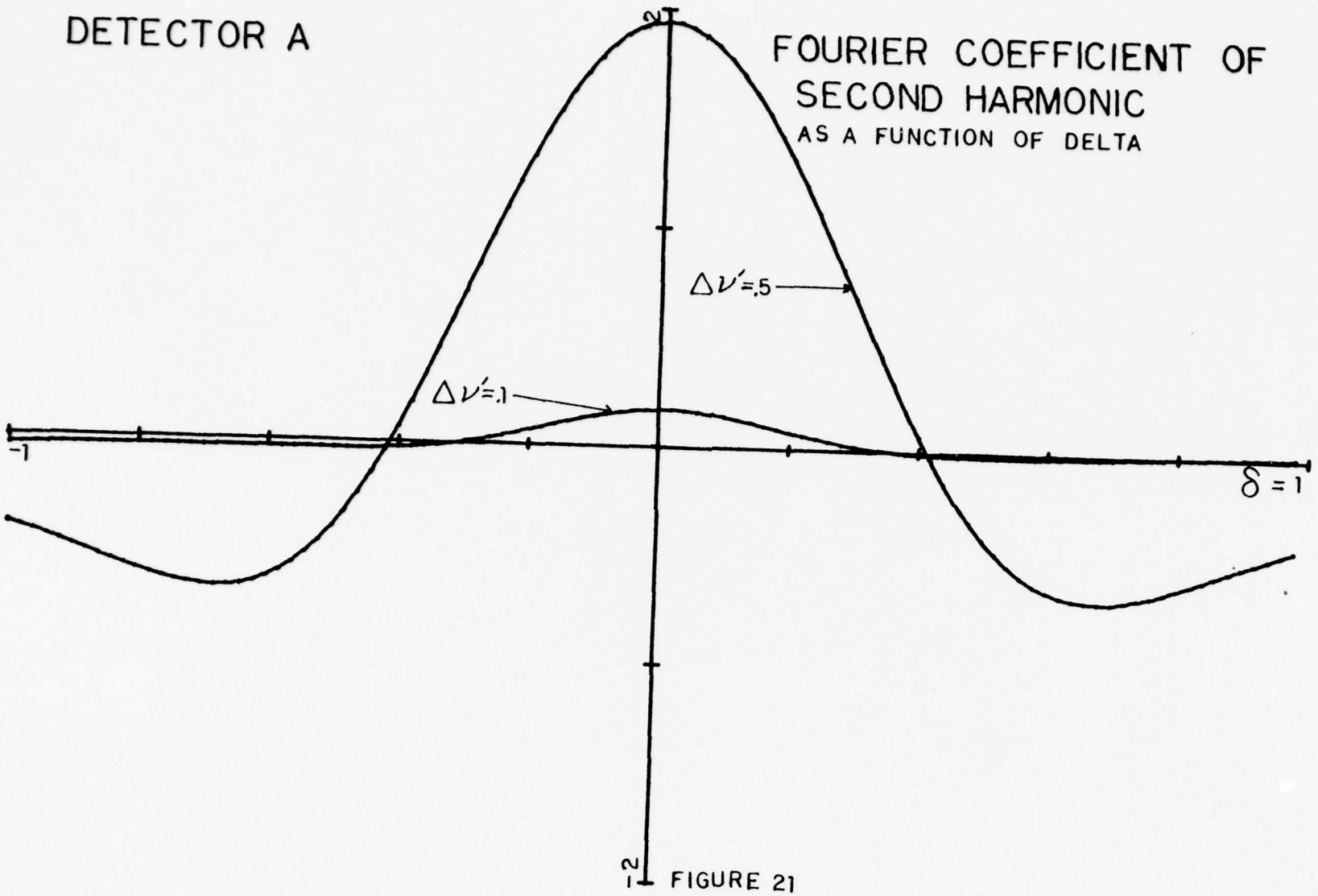
DETECTOR A
FOURIER COEFFICIENT OF
SECOND HARMONIC
AS A FUNCTION OF DELTA
Δν'=.5
Δν'=.1
-1
δ = 1
2
1

FIGURE 21

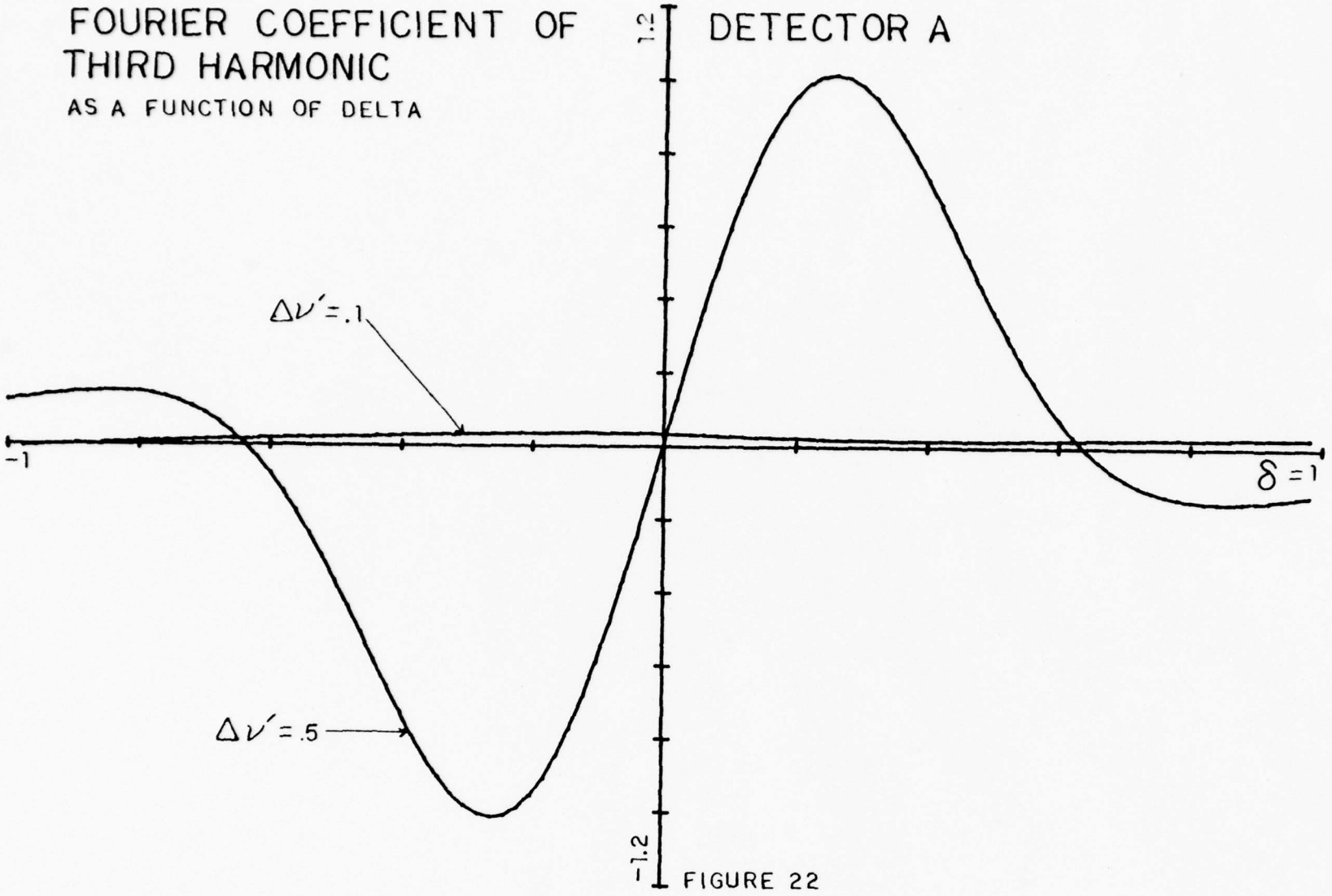
FOURIER COEFFICIENT OF DETECTOR A
THIRD HARMONIC
AS A FUNCTION OF DELTA
1.2
-1.2
-1
δ = 1
Δν' = .1
Δν' = .5

FIGURE 22

greater than the random variation of the laser frequency $\nu$.



bring the laser frequency back into the linear portion of the discriminant.

Figure 22 shows that the third harmonic may be used to produce an error signal if the dither amplitude is sufficiently large.

It is concluded that an error signal may be produced by phase sensitive detection of the fundamental or first harmonic of the detector signal. The lock-in amplifier establishes zero time from the reference signal. The phase of the detector harmonic will either be 0 or 180°. The polarity of the error signal is determined by the phase of the harmonic being monitored. The amplitude of the error signal is proportional to the amplitude of the harmonic, and for the first and third harmonics the error signal is linearly proportional to the frequency difference $\delta$ in the region near $\delta = 0$.

## E. ERROR SIGNAL ANALYSIS FOR A HgCdTe DETECTOR

Consider now using a nondifferentiating detector. The detector has an output voltage proportional to the absolute incident intensity. Such a detector would be a HgCdTe detector. This type of detector will be referred to as "detector B." With detector B in the loop the detector signal will be proportional to I(t) as given in (58). Equation (58) can be approximated to first order according to $e^x \cong 1 + x$ for x small. Thus the detector output voltage is proportional to (61) and should contain a large D.C.

term due to expanding the exponential. A plot of (61) as a function of time showed that this was indeed the case. The function is also an even function, i.e., $f(-t) = f(t)$; thus expansion is a Fourier cosine series and only the $a_n$'s in (65) need be calculated.

Plotting the coefficients of the harmonics as a function of $\delta$ as before should show whether or not detector B yields a suitable error signal. Plots for the first, second, and third harmonics are given in Figs. 23, 24, and 25. The results are similar to detector A. Phase sensitive detection of the first or third harmonic would yield an error signal. The second harmonic is unsuitable for error signal production.

## F. THE SERVO LOOP INTEGRATOR

It is desired to maintain the P(20) line in coincidence with the center frequency of a Stark shifted $NH_2D$ transition as accurately as possible. When the two transitions are in coincidence the error signal is zero. Using Fig. 19 as an example, consider a slight temperature increase in the cooling water. The laser cavity will expand and pull the oscillation to a lower frequency according to (45). This results in a negative $\delta$ and a positive error signal proportional to $\delta$ (assuming $\delta > -.2$ in Fig. 19). Feeding the error signal directly to the PZ supply then causes the supply to increase the PZ voltage and make a cavity length contraction correction. But as the cavity length returns

FOURIER COEFFICIENT OF
FIRST HARMONIC
AS A FUNCTION OF DELTA
DETECTOR B
$\delta = 1$
$\Delta\nu' = .1$
$\Delta\nu' = .5$

FIGURE 23

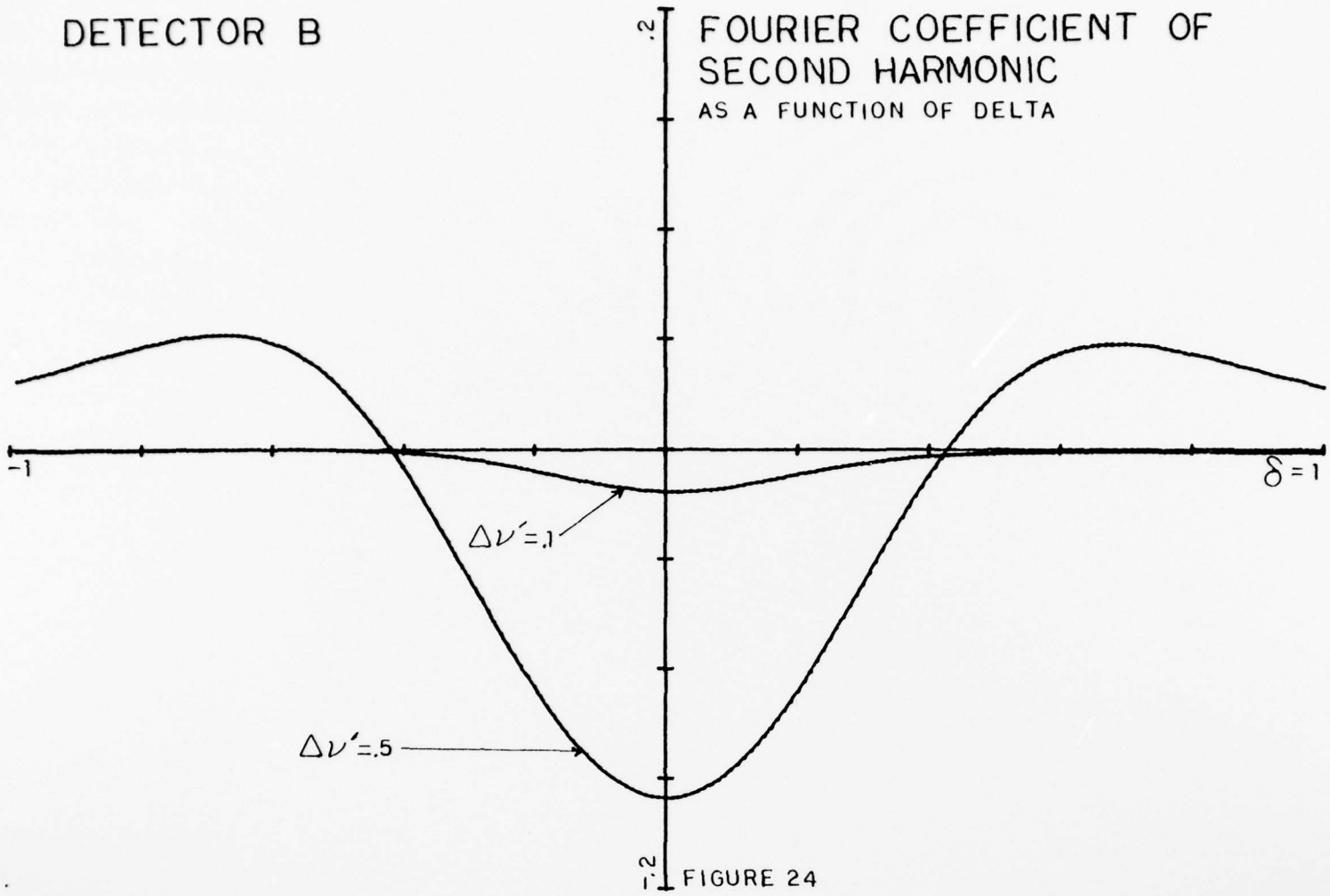
DETECTOR B
FOURIER COEFFICIENT OF SECOND HARMONIC
AS A FUNCTION OF DELTA
.2
-.2
-1
δ = 1
Δν'=.1
Δν'=.5

FIGURE 24

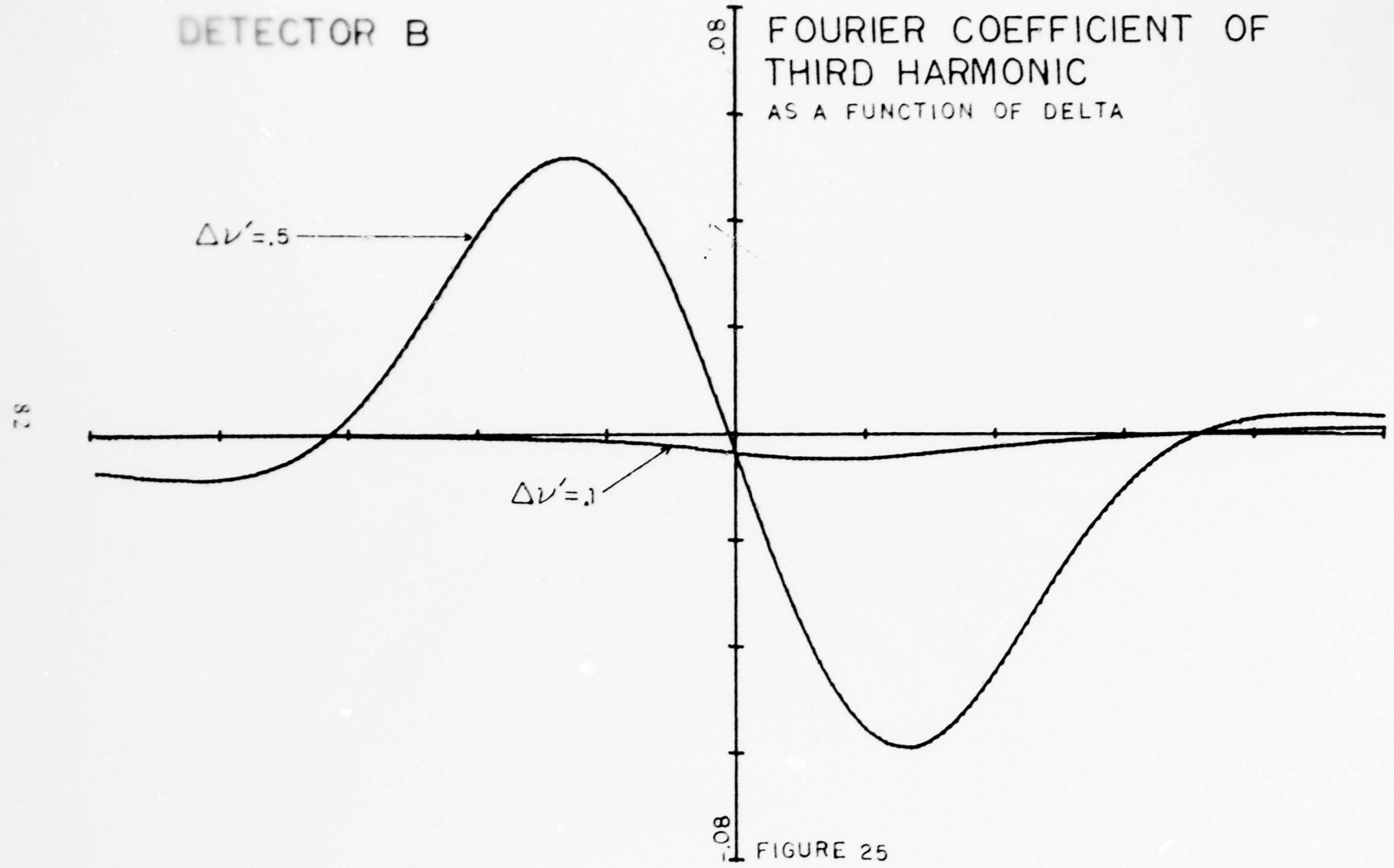
DETECTOR B
FOURIER COEFFICIENT OF THIRD HARMONIC
AS A FUNCTION OF DELTA
.08
-.08
Δν'=.5
Δν'=.1

FIGURE 25

to the original length the error signal decreases until an equilibrium point is reached at some finite nonzero $\delta$, such that the frequency difference $\delta$ produced by the PZ voltage produces just the right error signal to produce that PZ voltage. It is obvious that $\delta$ could never return to zero as the error signal would be zero indicating no length correction.

A method is needed to maintain the required PZ voltage as the error signal returns to zero. This could be accomplished by integrating in time the error signal produced by the lock-in and producing a new error signal to drive the PZ supply which is proportional to the total time integral of the first error signal. To the author's knowledge, the use of an integrator in the servo loop has not been mentioned before in the literature.

The integrator is placed between the lock-in amplifier and the PZ power supply as indicated in Fig. 6. Now as the error signal begins to return toward zero, the integrator continues to increase its output until the error signal is actually zero. At $\delta = 0$ the integrator maintains a constant D.C. output indefinitely or until a nonzero error signal indicates a need to change. If the error signal again went positive the integrator output increases still further, until a return to zero of the error signal indicates for the integrator to maintain a constant output at the new voltage reached.

If the error signal went negative the integrator would lower its output and continue to do so until the error signal actually returned to zero.

The ideal integrator would respond to both rapid and slow changes of the error signal. It would integrate rapidly enough so as to stabilize against acoustic vibrations yet also be able to accommodate slow changes in temperature. It should be designed to stabilize over the maximum temperature change expected and maximum pressure change expected. Such a device would produce a highly stable system suitable for operation in the field or in the laboratory.

## G. THE STARK CELL

Stabilization was never achieved due to numerous design problems in the Stark cell. Six different cells were made. These are discussed below.

### 1. Stark Cell One

The first Stark cell had stainless steel plates 10 cm long and 1.5 cm wide glued with plastic spacers into a plastic tube 1.7 cm I.D. Stainless leads fastened to the plates were sealed with glue through holes in the side of the tube. The cell was made to accommodate one-inch NaCl windows as were all the cells. The plate material was too thin and as the glue hardened on the leads, the plates warped.

2. Stark Cell Two

This was made with heavy stainless plate 10 cm long and 3 cm wide with a plate separation of 1.4 mm. The maximum observed D.C. modulation was 20% at a D.C. voltage of 490 volts and a pressure of 4.7 torr. The electric field was perpendicular to the laser polarization. The problem was that breakdown occurred at 500 volts. Also diffraction was a problem with the narrow plate separation.

3. Stark Cell Three

This was made with plates 20 cm long, 3.5 cm wide and about 3 mm thick. Care was taken to round the sides and corners of the plates. The plates were separated to 4 mm in an effort to eliminate breakdown and minimize diffraction. The cell had a gross air leak which could only be remedied by redesign. The cause of the leak was the rubber "O" rings.

4. Stark Cell Four

This was the same as above with slightly modified end window mounts. Slight modulation was obtained at 1400 volts at a pressure of 47 torr with the E field perpendicular to P. The intensity through the cell was .12 W. Breakdown also occurred at this potential. At lower pressures breakdown occurred at lower potentials.

It was then pointed out that in a low pressure gas electricity does not always take the shortest path. In fact, it was observed in this cell that at certain pressures

the discharge occurred between the outside two surfaces of the plates where the distance was greater rather than between the two inside surfaces. It is a fact that breakdown potential is not a function of distance but of pressure times distance. A plot of breakdown potential as a function of p x d is a skewed parabola with a minimum at some value of p x d. This value is called the pd minimum or Paschen minimum. To the right of the pd minimum breakdown potential increases with increasing pressure and distance as would normally be expected. But to the left of the pd minimum the breakdown potential decreases with increasing pressure and distance. Consequently if one is unfortunate in his choice of pressure and distances such that he is operating to the left of the pd minimum, increasing the plate separation will only make matters worse.

5. Stark Cell Five

The above cell was then disassembled and mylar was glued to the inside surfaces of the plates. All other exposed metal surfaces including the lead wires were coated with RTV silicone rubber. As the cell was placed under vacuum the glue and RTV began to outgas forming gas pockets on the plates and in the RTV. The required 1500 volt potential placed on the plates punched through the RTV and still resulted in breakdown.

The problem was reevaluated. The operating pressure could not be changed enough to solve the breakdown problem as the Stark effect ceases to give good modulation at too

high or too low a pressure [Ref. 18]. Two physical characteristics were desired which appeared to be mutually exclusive: a wide channel between the plates for ease of alignment and a minimum of diffraction, and the elimination of the breakdown problem.

6. Stark Cell Six

A completely new design approach was taken: to effectively place all metal surfaces outside of the cell, isolated from the low pressure gas filled channel. A 3 mm by 10 mm wide channel was cut in a solid 22 cm long block of plastic. The plates were embedded in the plastic on either side of the 3 mm width. The design called for 1 mm of plastic between each plate and the channel, resulting in a plate separation of 5 mm. Due to crazing of the 1 mm thick wall in the machining process, a film of mylar was added to the underside of each plate when they were embedded in the plastic. This resulted in an uneven plate separation of approximately 7 mm. The cell was tested to 3000 volts with no breakdown. It also held a good vacuum. However, it is anticipated that the uneven plate separation may result in a broadened or distorted absorption profile. Testing was not carried out further due to a permanent failure of the laser and its power supply.

This design appears to be the best approach. With this plate separation of 7 mm, wider plates should be used to minimize fringe effects of the electric field. Also the fabrication process needs to be modified so that the plates

are parallel, but sealed in plastic with no crazing in the high field areas. The plates should be thick so that the corners and edges can be rounded to minimize possible breakdown of the plastic. One solution might be to first cement a heavy plate to a block of plastic then machine the channel and cement the two halves together.

# IV. CONCLUSION

The instabilities of the Sylvania $CO_2$ Model 941 laser have been studied and the laser determined to be suitable for Stark cell stabilization. It was found that the existing unregulated, unfiltered laser power supply was unsuitable for a stabilized system and a new well regulated power supply needs to be purchased. Laser characteristics required to build a stabilized system such as piezoelectric parameter and thermal expansion coefficient have been measured. The optimum discharge current was found to be 7.5 mA. All the physical and operating characteristics of the laser pertinent to the design of a stabilized system have been studied and listed.

A computer analysis has been carried out to demonstrate the feasibility and production of an error signal with existing equipment. Both a Pyroelectric and HgCdTe detector are suitable for error signal production by phase sensitive detection of the first harmonic. A secondary result of the computer analysis was the demonstration of the need for a servo loop integrator. The purpose and operation of such an integrator was discussed. Theoretically the integrator should provide increased stability over that indicated thus far in the literature.

A Stark cell with no known major design flaws has been constructed and tested to 3000 volts with no breakdown. It

is vacuum tight to at least $10^{-5}$ torr. It is expected to be successfully used in the stabilization system.

All preliminary engineering studies have been carried out for assembling a Stark stabilized $CO_2$ laser system operating on the P(20) mode. This system will be operational in both the laboratory and the field.

## APPENDIX A

## MODEL 941 SYLVANIA LASER SPECIFICATIONS

Output wavelength: 10.6 μm

Power output: 3 watts

Beam divergence: 4 mrad

Beam diameter to 1/e point: 4 mm

Beam polarization: vertical

Cavity length: 45 cm

Bore diameter: ~ 6 mm

Cooling requirements: tap water @ 15 to 30 ml/s

Output mirror: 70% reflecting, dielectric flat

Piezoelectric mirror: 100% reflecting, 300 cm radius of curvature

Piezoelectric $\frac{\Delta L}{\Delta V}$ parameter

As given by Sylvania: $-4 \times 10^{-3}$ μm/volt

Measured: $-3.8 \times 10^{-3}$ μm/volt

Laser voltage: 14 kV @ 7.6 ma

Tube voltage: 9.5 kV @ 7.6 ma

Series ballast resistance: 600 kΩ

Equivalent tube resistance @ 7.6 ma: 1.27 MΩ

Pressure broadened linewidth: 100 MHz

Doppler broadened linewidth: 50 MHz

$\frac{c}{2L}$ mode separation: 333 MHz

Cavity linewidth: 19 MHz

## APPENDIX B

## STARK CELL SPECIFICATIONS

Two parallel plates totally encased in plastic with a 3 mm x 10 mm light beam channel at the axis of the cell between the plates. Channel is sealed off with one inch NaCl windows at each end and is vacuum tight. Channel is filled through one port.

Plate separation: 7 mm

Plate width: 3.6 cm

Plate length: 20.3 cm

# APPENDIX C

## HP 9810A CALCULATOR PROGRAM FOR THE VOIGT PROFILE

The Voigt profile is the convolution of a Lorentzian and a Gaussian profile. This HP 9810A program convolves numerically a Gaussian $g_1(x)$ and a Lorentzian $g_2(x)$ which have equal heights at the center frequency, i.e.,

$$g_1(\nu_o) = g_2(\nu_o) \ . \tag{C1}$$

Solving (C1) and setting $\nu_o = 0$ and $\frac{\Delta\nu}{2} = \frac{1}{\pi}$ the Gaussian and Lorentzian profiles are simplified to

$$g_1(x) = \exp\ [-\pi x^2]$$

and (C2)

$$g_2(x) = \frac{1}{[1 + (\pi x)^2]}$$

These were the equations plotted in Fig. 5. Equations (C2) are convolved according to

$$g(x) = \int_{x_{min}}^{x_{max}} g_1(y)\ g_2(x - y)\ dy \tag{C3}$$

The flow diagram and complete program are given on the following pages. The counter containing the value of n is register (000). The value of y is stored in (b), the value of x in (a). dx and dy are stored in (100). $1/\pi^2$ is stored in (099). (098) is a temporary storage for holding the previous value of f for the numerical integration routine. Registers (001) through (093) are reserved for storing $S_n$ where $S_n$ goes into (n). $x_{max}$ is stored in (097).

$n_{max} = \frac{x_{max} - x_{min}}{dx}$ is stored in (096). n + 1 is stored in (095) and A which is the normalizing factor is stored in (094). All registers should be cleared before beginning. Begin by prestoring these typical values:

$dx = dy = .1 \rightarrow (100)$

$x_{max} = -x_{min} = 4 \rightarrow (097)$

$n_{max} = 80 \rightarrow (096)$

$y = -4 \rightarrow (b)$

$x = -4 \rightarrow (a)$

$(\frac{\Delta\nu}{2})^2 = \frac{1}{\pi^2} \rightarrow (099)$

Set up the plotter for $x_{max} = 4$, $x_{min} = -4$ and $y_{max} = 1$, $y_{min} = 0$. Load the program and press continue. The computer will plot out the Voigt profile in approximately 20 minutes.

FLOW CHART

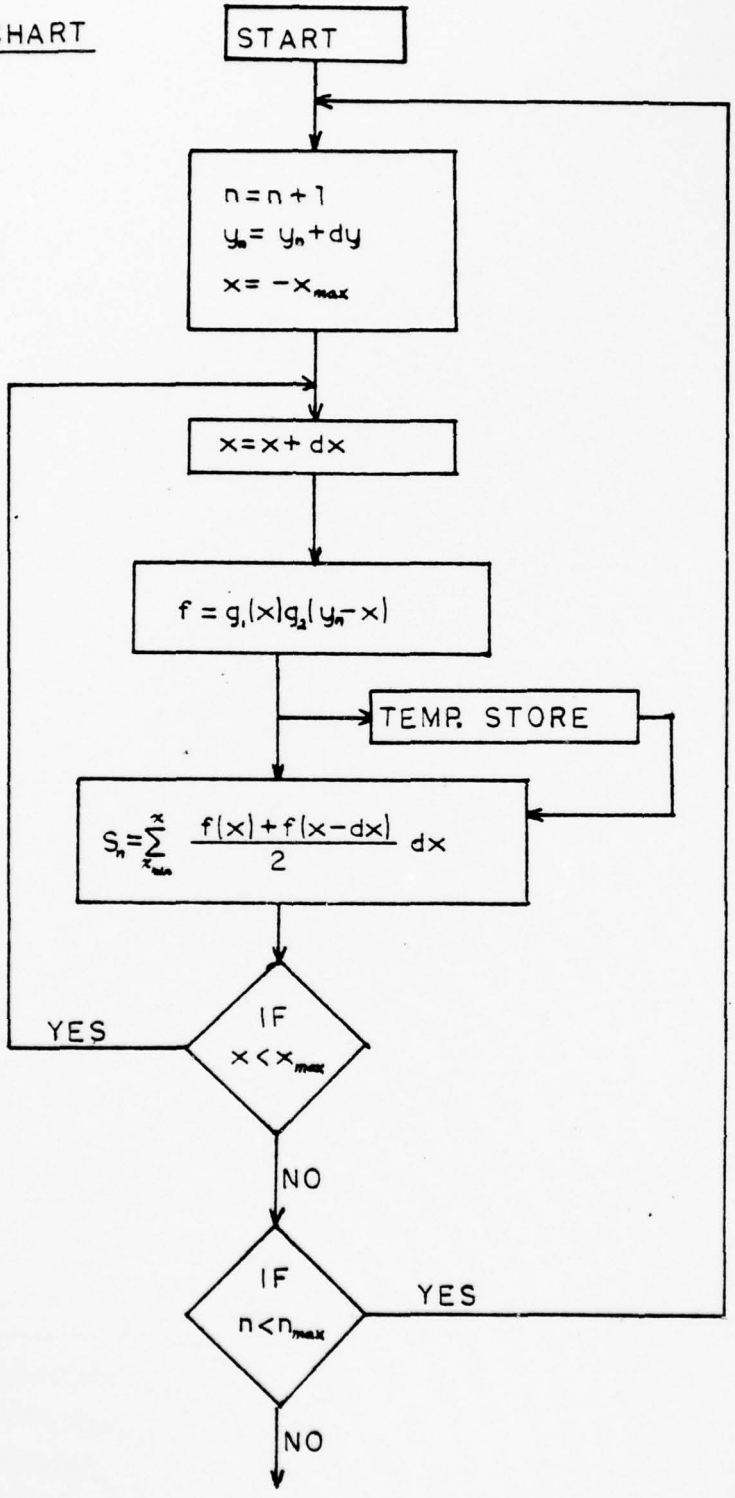
START
n = n + 1
$y_n = y_n + dy$
$x = -x_{max}$
x = x + dx
$f = g_1(x) g_2(y_n - x)$
TEMP. STORE
$S_n = \sum_{x_{min}}^{x} \frac{f(x) + f(x-dx)}{2} dx$
IF
$x < x_{max}$
YES
NO
IF
$n < n_{max}$
YES
NO

AD-A075 210 NAVAL POSTGRADUATE SCHOOL MONTEREY CA F/G 20/5
FREQUENCY CONTROL OF A CO2 LASER USING STARK CELL STABILIZATION--ETC(U)
JUN 79 D M BROW

UNCLASSIFIED NL

2 OF 2
AD A075210

END
DATE FILMED
11-79
DDC

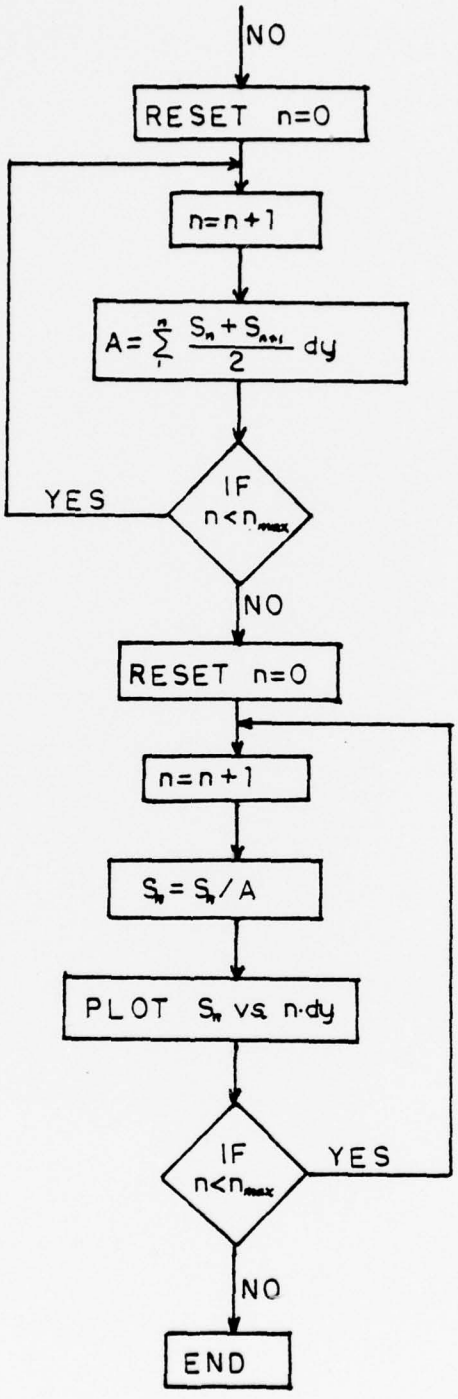
NO
RESET n=0
n=n+1
$A=\sum_{1}^{n}\frac{S_n+S_{n+1}}{2}dy$
IF $n<n_{max}$
YES
NO
RESET n=0
n=n+1
$S_n=S_n/A$
PLOT $S_n$ vs. n·dy
IF $n<n_{max}$
YES
NO
END

| STEP NO. | STEP |
|---|---|
| 0000 | CONTINUE |
| | 1 |
| | x → ( ) |
| | + |
| | 000 |
| | x → ( ) |
| | 100 |
| | x → ( ) |
| | + |
| | b |
| | x → ( ) |
| | 097 |
| | CHG SIGN |
| | x → ( ) |
| | a |
| 0021 | CONTINUE |
| | x → ( ) |
| | 100 |
| | x → ( ) |
| | + |
| | a |
| | a |
| | $x^2$ |
| | ↑ |
| | π |
| | ÷ |
| | x → ( ) |
| | 099 |
| | ÷ |
| | + |
| | CHG SIGN |
| | $e^x$ |
| | ↑ |
| | π |
| | $x^2$ |
| | ÷ |
| | b |
| | x → ( ) |
| | - |
| | a |
| | $x^2$ |
| | x → ( ) |
| | + |
| | 099 |
| | ÷ |
| | x → ( ) |
| | 098 |
| | y → ( ) |
| | 098 |
| | + |
| | 2 |
| | ÷ |
| | x → ( ) |
| | 100 |
| | x |
| | y → ( ) |
| | INDIRECT |
| | + |
| | 000 |
| | x → ( ) |
| | 097 |
| | ↑ |
| | a |
| | IF x < y |
| | 0021 |
| | x → ( ) |
| | 096 |
| | ↑ |
| | x → ( ) |

```
                000
                IF x < y
                0000
                0
                x ← ( )
                000
0109            CONTINUE
                1
                x ← ( )
                +
                000
                x ← ( )
                000
                ↑
                1
                +
                y ← ( )
                095
                x ← ( )
                INDIRECT
                000
                ↑
                x ← ( )
                INDIRECT
                095
                +
                2
                ÷
                x ← ( )
                100
                x
                y ← ( )
                +
                094
                x ← ( )
                096
                ↑
                x ← ( )
                000
                IF x < y
                0109
                0
                x ← ( )
                000
0170            CONTINUE
                1
                x ← ( )
                +
                000
                x ← ( )
                INDIRECT
                000
                ↑
                x ← ( )
                094
                ÷
                x ← ( )
                100
                ↑
                x ← ( )
                000
                x
                x ← ( )
                097
                -
                ↓
                FMT
                1
                ↓
                x ← ( )
```

```
096
↑
x ← ( )
000
IF x < y
0170
END
```

# APPENDIX D

## HP 9810A CALCULATOR PROGRAM FOR STARK FREQUENCY DISCRIMINANT

### I. FREQUENCY DISCRIMINANT FOR PYROELECTRIC DETECTOR

The following program plots $b_n$ in Eq. (66) as a function of $\delta$, where f(t) is given by (64) with S = 1 and $\Delta\nu = 1$. The first step in the program, K2, sets the calculator to work in radians. $\delta$ is prestored in (000), $\Delta\nu'$ is prestored in (006), and n (which determines the harmonic) is prestored in (007). The values of the constants A, B, C, D, and E in (64) are calculated and stored in registers (001), (002), (003), (004), and (005), respectively, in the program. The variable t is stored in (a) and dt in (b). (008) is a temporary store for the numerator in (64). (012) is a temporary store for the numerical integration routine. (010) accumulates the value of the integral in (66).

Begin with all registers cleared and the program loaded. Set up plotter for $-1 \leq x \leq 1$ and $-2 \leq y \leq 2$ or some other appropriate limits. Prestore -1 in register (000), .5 in (006), 1 in (007), .01 or .05 in (b). Press continue and Fig. 20 will be plotted out from left to right.

| STEP NO. | STEP | | |
|---|---|---|---|
| 0000 | K | | 8 |
| | 2 | | ÷ |
| | x ← ( ) | | ↓ |
| | 000 | | + |
| | $x^2$ | | 16 |
| | ↑ | | 1/x |
| | x | | + |
| | ↑ | | y → ( ) |
| | 3 | | 001 |
| | x | | 4 |
| | 4 | | CHG SIGN |
| | 1/x | | ↑ |
| | + | | x ← ( ) |
| | x ← ( ) | | 000 |
| | 006 | | $x^2$ |
| | $x^2$ | | x |
| | x | 0063 | 3 |
| | ↓ | 0064 | ↑ |
| | + | | x ← ( ) |
| | x ← ( ) | | 006 |
| | 000 | | $x^2$ |
| | $x^2$ | | x |
| | ↑ | | ↓ |
| | 2 | | - |
| | ÷ | | 1 |
| | ↓ | | - |
| | + | | x ← ( ) |
| | x ← ( ) | | 000 |
| | 006 | | x |
| | $x^2$ | | x ← ( ) |
| | $x^2$ | | 006 |
| | ↑ | | x |
| | 3 | | y → ( ) |
| | x | | 002 |

```
                x ← ( )
                000
                x²
                ↑
                3
                x
                4
                1/x
                +
                x ← ( )
                006
                x²
                ↑
                2
                ÷
                ↓
                +
                x ← ( )
                006
                x²
                x
                y → ( )
                003
                x ← ( )
                006
                ↑
                x²
                x
                x ← ( )
                000
                x
                y → ( )
0135            004
0136            x ← ( )
                006
                x²
                x²
                ↑
                8
                ÷
                y → ( )
                005
                0
                x → ( )
                a
0152            CONTINUE
                b
                x → ( )
                +
                a
                a
                ↑
                π
                x
                2
                x
                ↓
                sin x
                ↑
                x ← ( )
                000
                x
                a
                ↑
                π
                x
                4
                x
                ↓
                sin x
```

```
                    ↑
                    x ← ( )
                    006
                    ×
                    2
                    ÷
                    ↓
                    -
                    x ← ( )
                    006
                    ×
                    2
0195                ×
0196                y ← ( )
                    008
                    a
                    ↑
                    π
                    ×
                    8
                    ×
                    ↓
                    cos x
                    ↑
                    x ← ( )
                    005
                    ×
                    a
                    ↑
                    π
                    ×
                    6
                    ×
                    ↓
                    cos x
                    ↑
                    x ← ( )
                    004
                    ×
                    ↓
                    -
                    a
                    ↑
                    π
                    ×
                    4
                    ×
                    ↓
                    cos x
                    ↑
                    x ← ( )
                    003
                    ×
                    ↓
                    +
                    a
                    ↑
                    π
                    ×
                    2
                    ×
0252                ↓
0253                cos x
                    ↑
                    x ← ( )
                    002
                    ×
                    ↓
                    +
                    x ← ( )
                    001
```

```
+
x ← ( )
008
CHG SIGN
x ⇄ y
÷
a
↑
2
x
π
x
x ← ( )
007
x
↓
sin x
x
x ← ( )
012
y ← ( )
012
+
2
÷
b
x
y ← ( )
+
010
a
↑
1
IF x > y
0152
```

```
0321
0322
```

```
0
↑
y ⇄ ( )
010
2
x
x ← ( )
000
FMT
1
↓
.01
x ← ( )
+
000
0
x ← ( )
012
x ← ( )
000
↑
1
IF x > y
0002
END
```

```
0353
```

## II. FREQUENCY DISCRIMINANT FOR HgCdTe DETECTOR

The following program plots $a_n$ in Eq. (65) as a function of $\delta$, where f(t) is given by (61) with S = 1 and $\Delta\nu$ = 1. As before (000), (006), (007), and (b) contain the appropriate prestored values. In the program (011) is the numerical integration routine temporary storage register and (009) accumulates the value of the integral.

| STEP NO. | STEP |
|---|---|
| 0000 | K |
| | 2 |
| 0002 | CONTINUE |
| | .01 |
| | x → ( ) |
| | + |
| | 000 |
| | 0 |
| | x → ( ) |
| | a |
| 0014 | CONTINUE |
| | b |
| | x → ( ) |
| | + |
| | a |
| | a |
| | ↑ |
| | 2 |
| | x |
| | π |
| | x |
| | ↓ |
| | cos x |
| | ↑ |
| | x ← ( ) |
| | 006 |
| | x |
| | x ← ( ) |
| | 000 |
| | $x \overset{\rightarrow}{\leftarrow} y$ |
| | - |
| | ↓ |
| | $x^2$ |
| | ↑ |
| | 4 |
| | 1/x |
| | + |
| | π |
| | x |
| | 2 |
| | x |
| | ↓ |
| | 1/x |
| | ↑ |
| | a |
| | ↑ |
| | 2 |
| | x |
| | π |
| | x |
| | x ← ( ) |
| | 007 |
| | x |
| | ↓ |
| | cos x |
| | x |
| | x ← ( ) |
| | 011 |
| | y → ( ) |
| | 011 |
| | + |
| | 2 |
| | ÷ |
| | b |
| | x |
| | y → ( ) |
| | + |
| | 009 |

```
              a
              ↑
              1
              IF x > y
              0014
              0
              ↑
              y ⇄ ( )
              009
              2
              ×
              x ← ( )
              000
              FMT
              1
              ↓
              0
              x → ( )
              011
              x ← ( )
              000
              ↑
              1
              IF x > y
              0002
0123          END
```

## APPENDIX E

## LOW PASS L-SECTION FILTER

Below is a schematic of the simple filter added to the high voltage D.C. laser power supply to reduce the 60 Hz current ripple. The filter consisted of a .5 microfarad 16 kilovolt capacitor and a 45 Henry choke which was actually the secondary winding of a 13 kV transformer. Since the input voltage was 15 kV, the transformer, being insulated for 2000 volts less, was isolated from ground on plastic supports. The filter successfully reduced the 60 Hz ripple in the power supply output by a factor of 50.

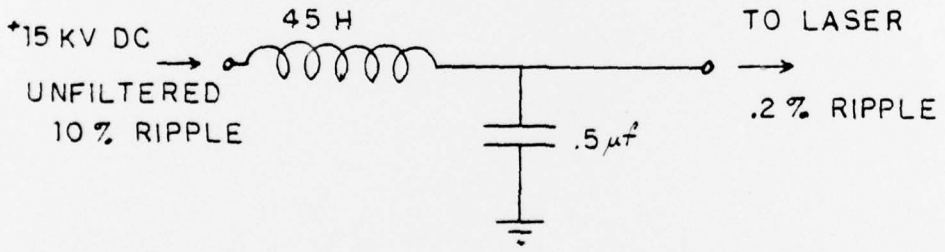

## APPENDIX F

## COPPER CONSTANTAN THERMOCOUPLE TEMPERATURE VS. E.M.F.

The following table gives values of thermocouple temperature and voltage with reference to ice water.

| E.M.F. (mV) | Temperature (°C) |
|---|---|
| 0 | 0 |
| .1 | 2.61 |
| .2 | 5.17 |
| .3 | 7.72 |
| .4 | 10.28 |
| .5 | 12.78 |
| .6 | 15.33 |
| .7 | 17.83 |
| .8 | 20.33 |
| .9 | 22.78 |
| 1.0 | 25.28 |
| 1.1 | 27.72 |
| 1.2 | 30.11 |
| 1.3 | 32.56 |
| 1.4 | 35.00 |
| 1.5 | 37.39 |
| 1.6 | 39.78 |
| 1.7 | 42.11 |
| 1.8 | 44.50 |
| 1.9 | 46.83 |
| 2.0 | 49.17 |

## APPENDIX G

## RELATIONSHIP OF TUBE WALL TEMPERATURE TO COOLING WATER OUT TEMPERATURE

The laser discharge region between the cavity mirrors is a pyrex glass tube .7 cm O.D. and 34.3 cm long surrounded by a glass water jacket 3 cm I.D. It is desired to find the average wall temperature of the .7 cm discharge tube knowing the bulk water temperature out. Reference 24 is used for this calculation. The problem is an annular tube flow type. It is assumed that the outer water jacket tube is at the bulk water temperature and that no heat flows through it to the surrounding air.

The following parameters are given, through experimental measurement or a handbook of physical constants.

flow rate: 14.6 ml/s

inlet temp.: 22.1°C

outlet temp.: 23.8°C

voltage across tube and balast resistor: 14 kV

voltage across tube: 9.5 kV

tube current: 7.6 mA

laser power output: 3 watts

specific heat of water: $C_p = 1$ cal/g-C°

density of water: $\rho = 1$ g/cm$^3$

viscosity of water at 22°C: $\mu = .009403$ g/cm-s

thermal conductivity of water at 0°C: $k_w = .001348$ cal/cm-s-°C

thermal conductivity of water at 40°C: $k_w = .001499$ cal/cm-s-°C

thermal conductivity of pyrex: $k_g = .0026$ cal/cm-s-°C

hydraulic diameter $2(r_o - r_i)$: $D_e = 2.3$ cm

tube surface area" $A_s = \pi(.7 \text{ cm})(34.3 \text{ cm}) = 75.4 \text{ cm}^2$

1. Determine if the flow is laminar or turbulent by calculating the Reynolds number.

   cross sectional area of water: $A = \pi(r_o^2 - r_i^2) = 6.68 \text{ cm}^2$

   velocity of water: $V = \frac{14.6 \text{ ml/s}}{6.68 \text{ cm}^2} = 2.19 \text{ cm/s}$

   $$Re = \rho\frac{VD_e}{\mu} = \frac{(1 \text{ g/cm}^3)(2.19 \text{ cm/s})(2.3 \text{ cm})}{.009403 \text{ g/cm-s}} = 536$$

   $\therefore$ Flow is definitely laminar.

2. Determine Nusselt number for laminar flow in a circular tube annulus, using [24].

   $$r^* = \frac{r_i}{r_o} = .23$$

   $$Nu_i = 8.212$$

3. Find the heat added to the water by the laser discharge tube only. This is approximately equal to the voltage across the tube times the current minus the power output.

   $$\frac{dQ}{dt} = (9.5 \times 10^3)(7.6 \times 10^{-3}) - 3 = 69.2 \text{ watts} = 16.54 \text{ cal/s}$$

4. Find the temperature difference $\Delta T$ across the tube and the bulk water temperature given the temperature out.

$$\frac{dQ}{dt} = C_p \, \Delta T \, \frac{dm}{dt}$$

$$16.54 \text{ cal/s} = \left(1 \frac{\text{cal}}{\text{g-C}^\circ}\right) \Delta T \, (14.6 \text{ g/s})$$

$$\Delta T = 1.1 \text{ C}^\circ$$

$$T_b = \frac{T_o + T_i}{2} = \frac{T_o + (T_o - 1.1)}{2} = T_o - \frac{1.1}{2}$$

5. The surface coefficient of the inner tube is found from the Nusselt number according to

$$h_s = \frac{k_w \, Nu_i}{D_e}$$

6. The rate of heat transfer through a .5 mm glass tube wall with an inside surface temperature $Tw_i$ and an outside surface temperature $Tw_s$ is given by

$$\frac{dQ}{dt} = k_g \, A_s \left(\frac{Tw_i - Tw_s}{.05 \text{ cm}}\right)$$

$$16.54 \frac{\text{cal}}{\text{s}} = \left(.0026 \frac{\text{cal}}{\text{cm-s-}^\circ\text{C}}\right)(75.4 \text{ cm}^2)(Tw_i - Tw_s)/.05 \text{ cm}$$

$$Tw_i - Tw_s = 4.2 \text{ C}^\circ$$

7. Derive a general formula for the average tube wall temperature given that the rate of heat transfer through the tube wall equals the rate through the surface layer equals the rate dissipated by the water.

$$\frac{dQ}{dt} = k_g A_s \frac{Tw_i - Tw_s}{.05} - h_s A_s (Tw_s - T_b) = C_p \Delta T \frac{dm}{dt}$$

$$Tw_A = \frac{Tw_i + Tw_s}{2}$$

From the above it is easily shown that

$$Tw_A = \frac{1}{2} \left(\frac{.05}{k_g A_s}\right) \frac{dQ}{dt} + \left(\frac{1}{h_s A_s}\right) \frac{dQ}{dt} + T_b$$

Substitution of the equations for $T_b$ and $h_s$ in 4 and 5 into this equation yields

$$Tw_A - \frac{1}{2} \left(\frac{.05}{k_g A_s}\right) \frac{dQ}{dt} + \left(\frac{D_e}{k_w Nu_i A_s}\right) \frac{dQ}{dt} + T_o - \frac{1.1}{2}$$

or

$$Tw_A = 1.56 + \frac{.0597}{k_w} + T_o$$

$$= 45.8° + T_o \text{ @ } 0°C$$

$$= 41.4° + T_o \text{ @ } 40°C$$

Clearly this proves that $\Delta Tw_A \cong \Delta T_o$.

## APPENDIX H

## PHOTOGRAPHS OF EQUIPMENT

Figure (H-1) is a photograph of the whole experimental setup. The L-section filter is on top of the laser power supply in the lower right-hand corner. The cooling water temperature control, filter, and regulator are at the sink in the upper right-hand corner.

Figure (H-2) is a photograph of the oscilloscope and rack-mounted instruments. From top to bottom the instruments in the rack are: audio power amplifier, lock-in amplifier, 3kV D.C. power supply, 2kV D.C. power supply, audio oscillator, and nonovoltmeter.

Figure (H-3) is a photograph of the laser and optical components. The laser is middle right in the photograph. Note the thermometer and thermocouple in the coolant tube coming out of the rear of the laser. The gas bottles and dewar for the thermocouple ice bath are at the bottom of the photograph. From the laser counterclockwise are: the chopper, beam splitter, spectrum analyzer, Stark cell, and pyroelectric detector.

Figure (H-4) is a photograph of the Stark cell. From left to right are: the beam splitter, chopper motor, laser, Stark cell, and detector. Note that the chopper motor is acoustically isolated from the table with a metal bar supported directly to the floor.

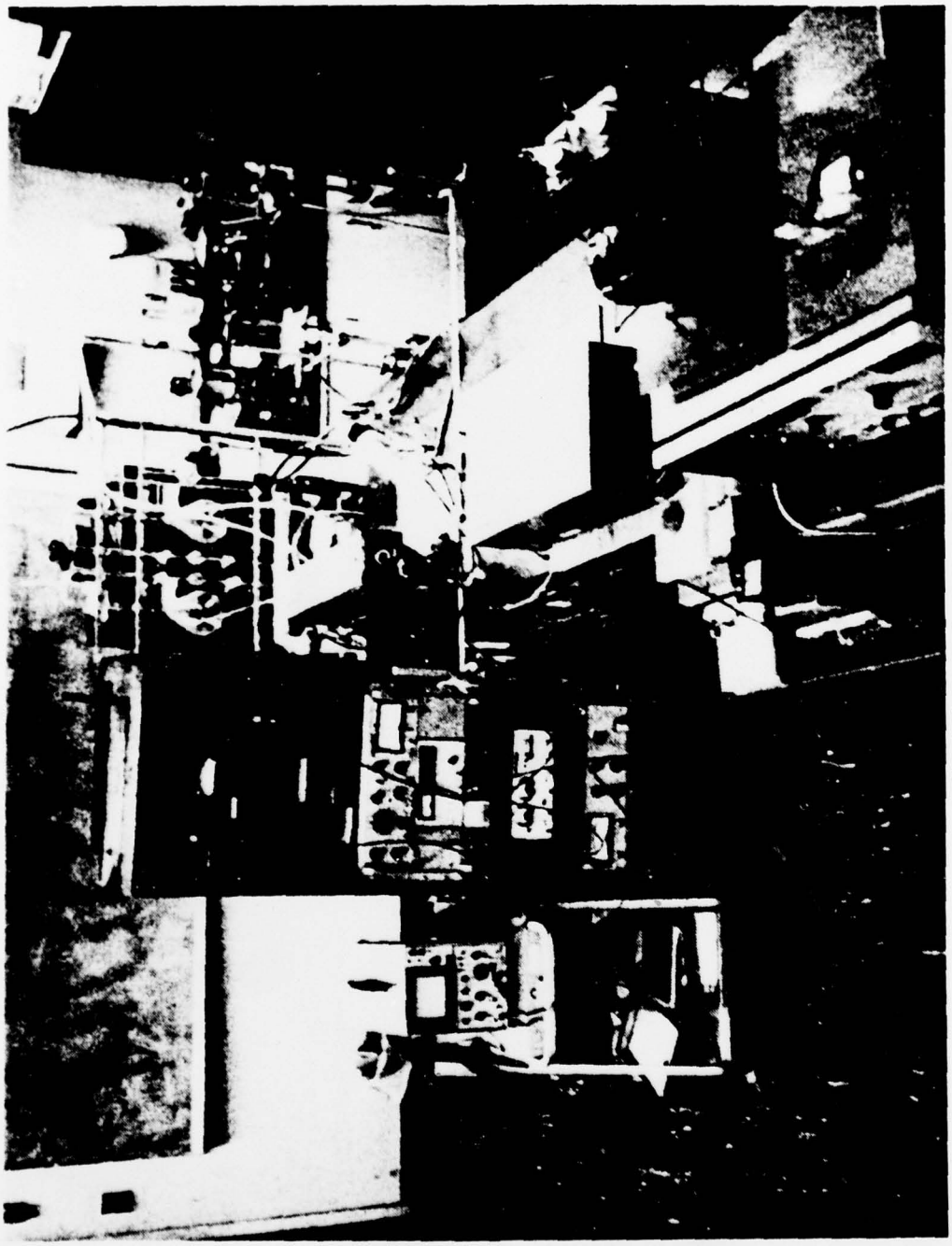

FIGURE H-1

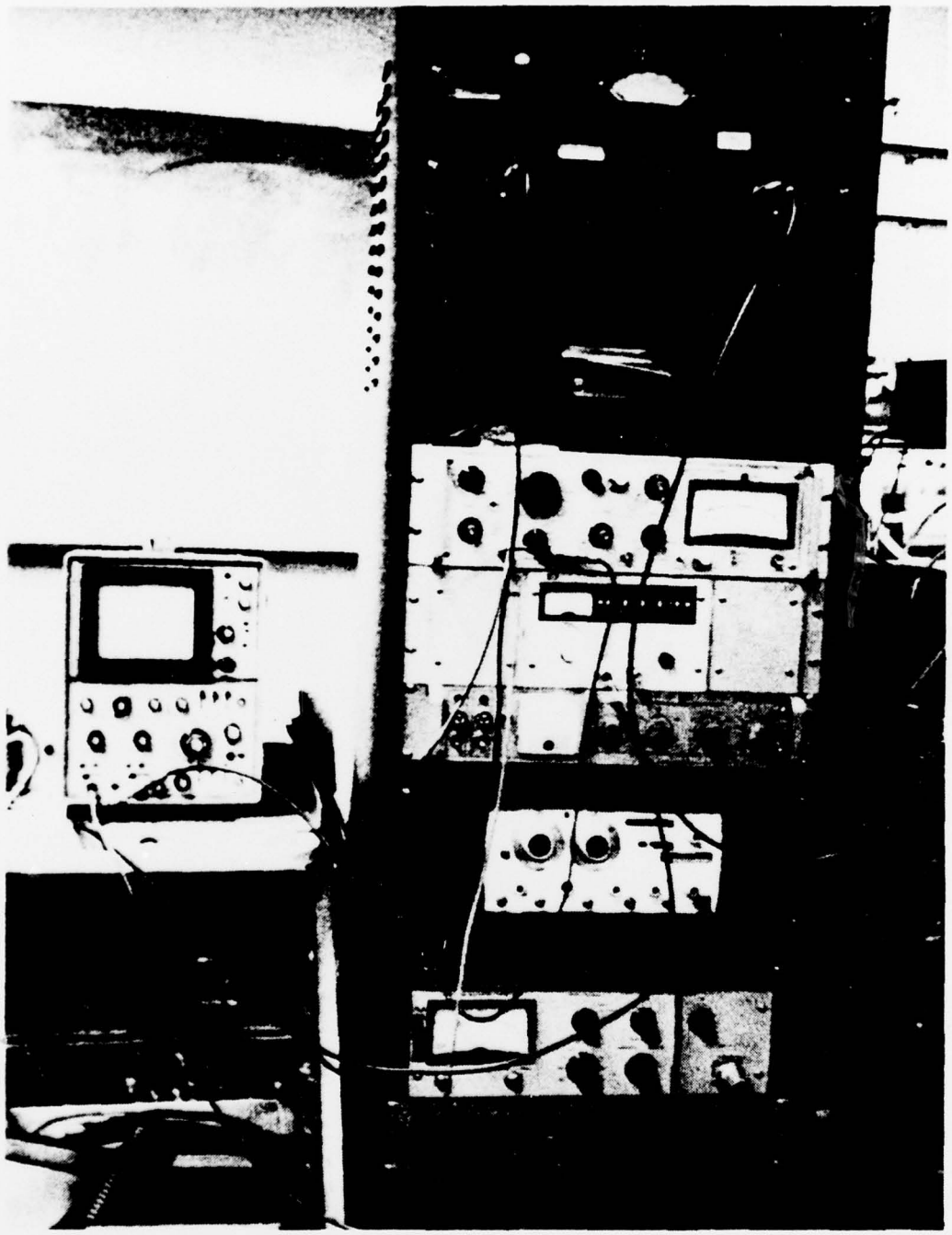

FIGURE H-2

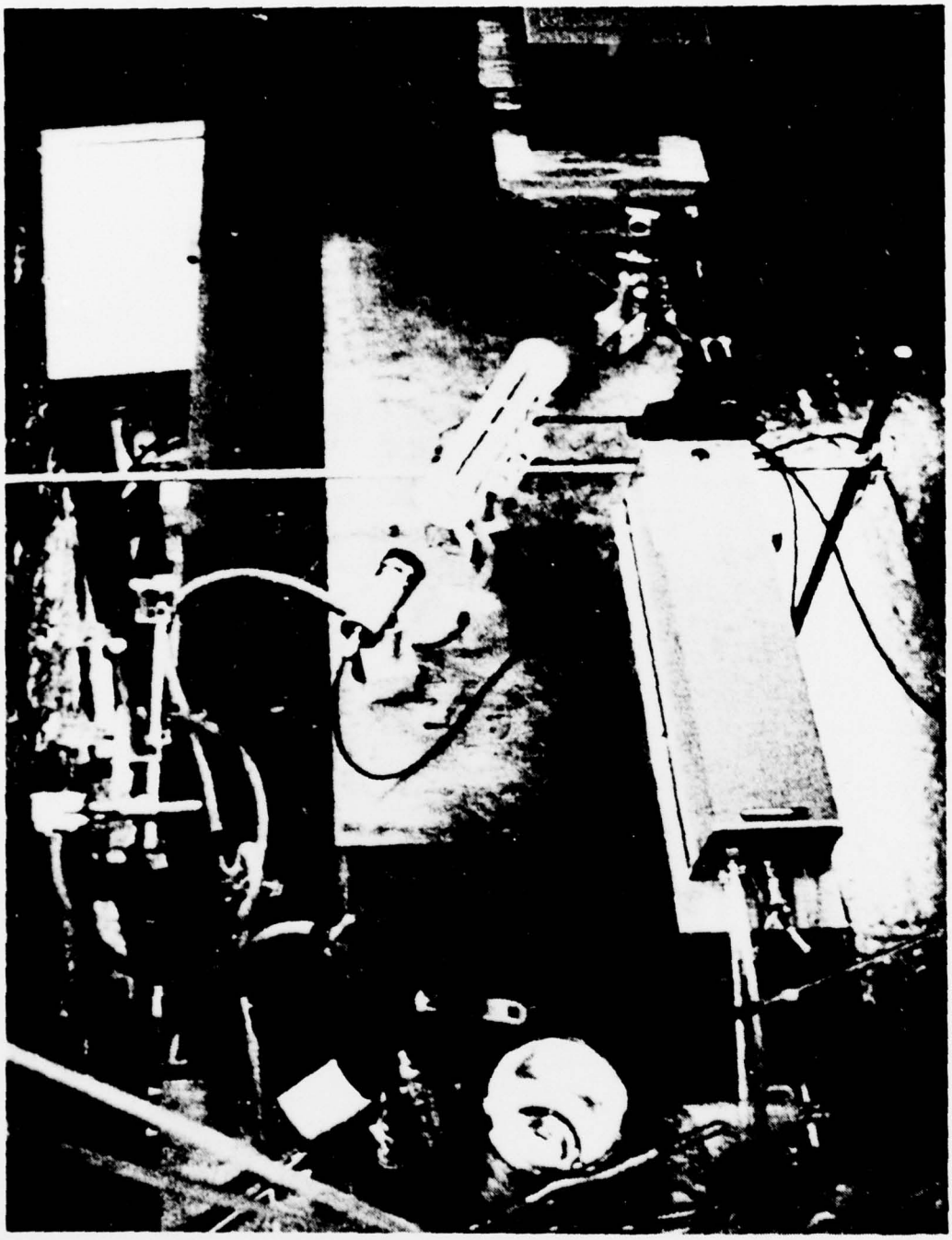

FIGURE H-3

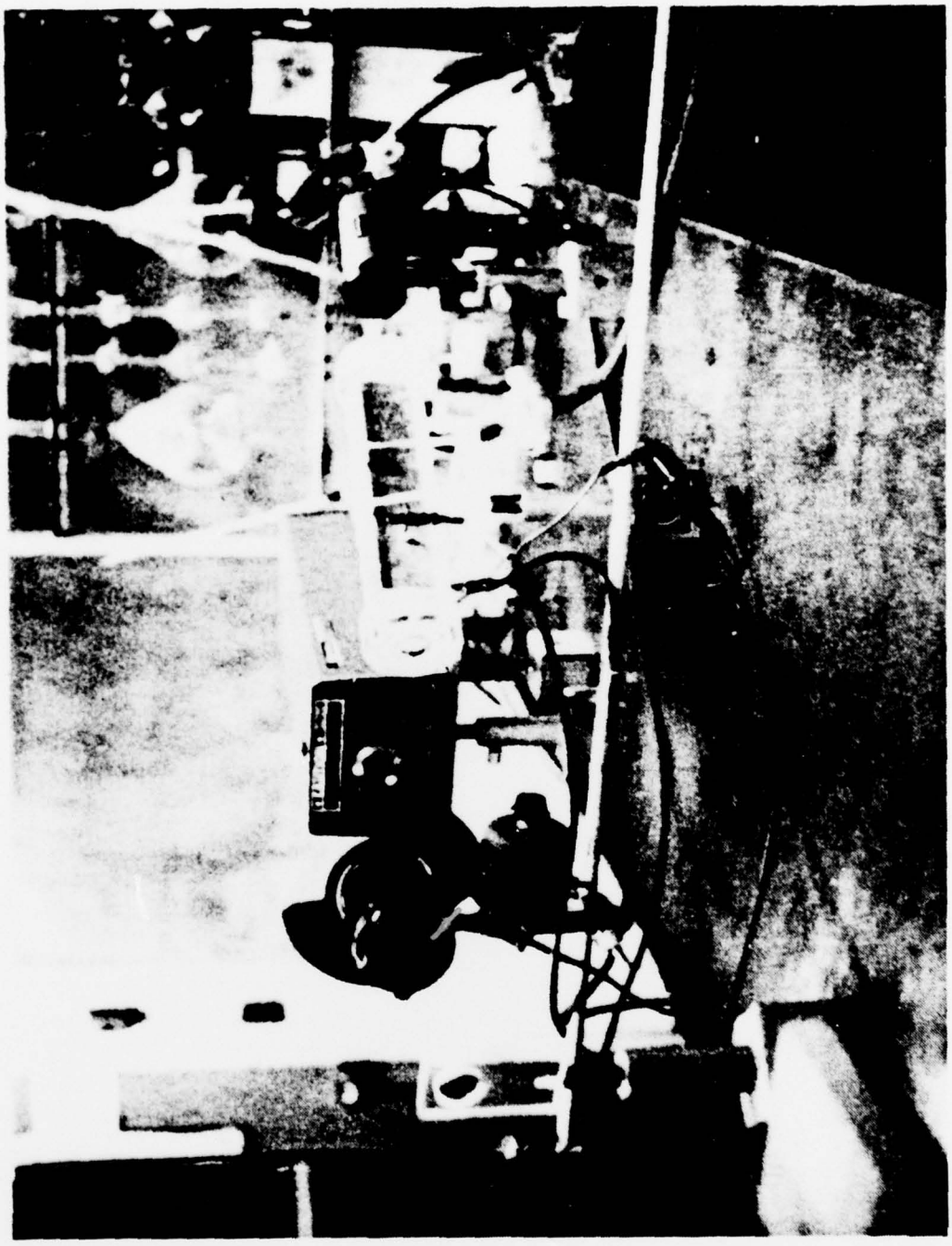

FIGURE H-4

## LIST OF REFERENCES


1. Tyte, D. C., "Carbon Dioxide Lasers," Advances in Quantum Electronics I, ed. D. W. Goodwin, pp. 129-198, Academic Press, 1970.

2. Herzberg, G., "Infrared and Raman Spectra," Molecular Spectra and Molecular Structure, Vol. 2, pp. 370-399, Van Nostrand Reinhold Company, 1945.

3. Yariv, A., Introduction to Optical Electronics, 2nd Ed., pp. 75-94, 113-118, Holt Rinehart and Winston, 1976.

4. Svelto, O., Principles of Lasers, p. 50, Plenum Press, 1976.

5. Thomas, J. B., Statistical Communications Theory, p. 58, Wiley, 1969.

6. Griem, H. R., Plasma Spectroscopy, p. 101, McGraw-Hill, 1964.

7. Townes, C. H. and Schawlaw, A. L., Microwave Spectroscopy, p. 375, McGraw-Hill, 1955.

8. Bloom, A. L., Gas Lasers, pp. 69-100, Wiley, 1968.

9. Kogelnik, H. and Li, T., "Laser Beams and Resonators," Applied Optics, Vol. 5, No. 10, pp. 1550-1567, October 1966.

10. Freed, C., "Design and Short-Term Stability of Single-Frequency $CO_2$ Lasers," IEEE Journal of Quantum Electronics, Vol. QE-4, No. 6, pp. 404-408, June 1968.

11. Mocker, Hans W., "A 10.6 μ Optical Heterdyne Communication System," Applied Optics, Vol. 8, No. 3, pp. 677-684, Mar 1969.

12. Bridges, T. J. and Patel, C. K. N., "High-Power Brewster Window Laser at 10.6 Microns," Applied Physics Letters, Vol. 7, No. 9, pp. 244-245, 1 Nov 1965.

13. Mocker, Hans W., "Pressure and Current Dependent Shifts in the Frequency of Oscillation of the $CO_2$ Laser," Applied Physics Letters, Vol. 12, No. 1, pp. 20-23, 1 January 1968.

14. Sinclair, D. C. and Bell, W. E., Gas Laser Technology, pp. 109-112, Holt, Rinehart and Winston, 1969.

15. Kelly, M. J., Francke, R. E., and Feld, M. S., "Rotational-Vibrational Spectroscopy of $NH_2D$ Using High-Resolution Laser Techniques," Journal of Chemical Physics, Vol. 53, pp. 2979-2980, 1970.

16. Martin, J. M., Corcoran, V. J., Smith, W. T., "Identification of Absorption Lines in Gases Used to Modulate the $CO_2$ Laser," IEEE Journal of Quantum Electronics, Vol. QE-10, pp. 191-195, February 1974.

17. Brewer, R. G., Kelly, M. J., Javan, A., "Precision Infrared Stark Spectra of $NH_2D$ Using Lamb Dip," Physical Review Letters, Vol. 23, No. 11, pp. 559-563, Sept 1969.

18. Claspy, P. C., and Pao, Yoh-han, "Basic Characteristics of High-Frequency Stark-Effect Modulation of $CO_2$ Lasers," IEEE Journal of Quantum Electronics, Vol. QE-7, No. 11, pp. 512-519, Nov 1971.

19. Nussmeier, T. A., and Abrams, R. L., "Stark Cell Stabilization of $CO_2$ Laser," Applied Physics Letters, Vol. 25, pp. 615-617, Nov 1974.

20. Tangonan, G. L. and Abrams, R. L., "Stark-tuned resonances of $N^{15}H_2O$ with $CO_2$ laser lines," Applied Physics Letters, Vol. 29, pp. 179-181, Aug. 1976.

21. Johnston, A. R. and Melville, R. D. S., "Stark-Effect Modulation of a $CO_2$ Laser by $NH_2D$," Applied Physics Letters, Vol. 19, pp. 503-506, Dec 1971.

22. Fork, R. L., Tomlinson, W. J., and Heilos, L. J., "Hysteresis in an He-Ne Laser," Applied Physics Letters, Vol. 8, No. 7, pp. 162-163, April 1966.

23. Carlson, Bruce A., Communications Systems, p. 247-249, McGraw-Hill, Second Ed., 1975.

24. Rohsenow, Warren M. and Hartnett, James P., Handbook of Heat Transfer, pp. 7-71 to 7-86, McGraw-Hill, 1973.

INITIAL DISTRIBUTION LIST

| | | No. Copies |
|---|---|---|
| 1. | Defense Documentation Center<br>Cameron Station<br>Alexandria, Virginia 22314 | 2 |
| 2. | Library, Code 0142<br>Naval Postgraduate School<br>Monterey, California 93940 | 2 |
| 3. | Department Chairman, Code 61 Wh<br>Department of Physics and Chemistry<br>Naval Postgraduate School<br>Monterey, California 93940 | 2 |
| 4. | Professor Alfred W. Cooper, Code 61 Cr<br>Department of Physics and Chemistry<br>Naval Postgraduate School<br>Monterey, California 93940 | 4 |
| 5. | Professor E. C. Crittenden, Jr., Code 61 Ct<br>Department of Physics and Chemistry<br>Naval Postgraduate School<br>Monterey, California 93940 | 1 |
| 6. | Mr. Morris A. Brown, Vice President<br>H. J. Gruy & Associates<br>2501 Cedar Springs Road<br>Dallas, Texas 75201 | 1 |
| 7. | Commandant (G-PTE)<br>U.S. Coast Guard<br>Washington, D.C. 20590 | 2 |
| 8. | LT Daniel M. Brown, USCG<br>Commandant (EOE)<br>U.S. Coast Guard<br>Washington, D.C. 20590 | 2 |